DESIGN AND ANALYSIS OF A TENSEGRITY ROBOT

A Final Year Project Report

Presented to

SCHOOL OF MECHANICAL & MANUFACTURING ENGINEERING

Department of Mechanical Engineering

NUST

ISLAMABAD, PAKISTAN

In Partial Fulfilment

of the Requirements for the Degree of

Bachelors of Mechanical Engineering

---

by

Abdul Muhaimin Pandhiani

Mahnoor Bilal

Saad Shabeer

June 2021

EXAMINATION COMMITTEE

We hereby recommend that the final year project report prepared under our supervision by:

ABDUL MUHAIMIN PANDHIANI	00000237557
MAHNOOR BILAL	00000214345
SAAD SHABEER	00000211143

Titled: "**DESIGN AND ANALYSIS OF A TENSEGRITY ROBOT**" be accepted in partial fulfilment of the requirements for the award of BE Mechanical Engineering degree with grade ___

Supervisor: Dr. Aamir Mubashar, (Professor)	Dated:
Co-Supervisor: Dr. Jawad Aslam, Assistant Professor	Dated:

_____ _____

(Head of Department) (Date)

COUNTERSIGNED

Dated: _____ _____

(Dean / Principal)

ABSTRACT

The curiosity of the human mind has led to many wonderful discoveries and inventions. This natural curiosity has led us to explore space to find and learn more about our place in the universe. Space has always been a puzzling subject and hence as human nature is, it is often an inquisitive topic for us.

Since achieving spaceflight, we have been able to produce societal benefits that improve the quality of life on earth, ranging from solar panels to implantable heart monitors, from cancer therapy to light- weight materials, and from water-purification systems to improved computing systems and to global search-and-rescue systems. It will continue to be an essential driver in opening up avenues in science and technology with more research and development in every sector.

Experience has demonstrated that, as long as humankind addresses the challenges of exploring mankind's common frontier of space, many tangible societal benefits are produced, and in addition to those most commonly anticipated, a great variety of valuable innovations are generated coincidentally, for this is the nature of discovery.

Pakistan has not contributed to space exploration in a long time, and we felt that it is the right time for young engineers of a developing country to take a step in this direction and quite frankly, this is the right challenge for us as engineers about to enter our fields.

With the current space research focused on tensegrity robots: structures that maintain a stable volume in space through the use of discontinuous compressive elements (struts) connected to a continuous network of tensile elements, the extracted data and results look promising enough to replace rovers with tensegrity robots for planet exploration in the future [1].

We have worked on the design and analysis of a six-strut tensegrity robot making use of morphological computation for actuation. The robot has been designed for Titan, Saturn's

largest moon. Its unique morphology allows it to withstand the huge impact loads without the need for airbags or similar landing accessories, and the actuation is made possible through utilizing morphological computation which significantly reduces the computational power needed.

ACKNOWLEDGMENTS

We are, first and foremost, and undoubtedly, grateful to Allah Almighty for giving us the strength, good health, and the opportunity to undertake this project.

Final Year Projects, like other long-term projects, are never the culmination of the efforts of just the team members. They are, and always will be, other people, albeit behind the curtains, who make such endeavours possible.

Recognizing our families: our parents who made sure that we kept the project's end in mind by regularly asking us "kitna aur rehta hai ye project??", comforted us when we were frustrated, brought us delicious food to enjoy, made sure we never worried about our basic needs as well as luxurious wants, supported us with their prayers, put up with our regular late-night meetings and much, much more. Our siblings (Muttaqi & Sheraz – for letting Muhaimin work in peace and distracting him from the project when he needed it; Maham – for distracting Mahnoor from the project's stress by assigning household chores; Humna – for thinking that Mahnoor was studying for the exams when she was in the FYP meetings; Mahad – for scaring Mahnoor on multiple on occasions while she was on call, providing valuable entertainment to Muhaimin and Saad; Mah Rukh – for regularly reminding Saad to do well in the project because "naak nahi katni chaye") were also important motivators during the course of this project.

We were also fortunate to have Dr. Aamir Mubashar and Dr. Jawad Aslam as our supervisors. They gave us freedom to work on a project that fascinated us from the very beginning, no matter how unorthodox; they gave us room to be creative with our project's direction and to challenge ourselves yet, providing us with valuable technical feedback whenever we were stuck in a rut. They always knew when to push and when to motivate. They encouraged us to step back and recognize our efforts, hard work and accomplishments in this project: giving us the perspective, whenever we would lose sight of it – making us feel much better at the end of any tough period. In parallel, they pushed

us to achieve more with our project and helped us learn more than we could have otherwise. We are especially grateful to Dr. Aamir, who put up with us during many of our gloomy and perhaps disorienting meetings, when we had lost our direction and our motivation; he provided us with the clarity, self-confidence, and energy that we needed-most at those times.

It would be unfair to not recognize Faraz Hussain and Sunia Tanweer for the valuable comic relief they provided us with over the course of this project as well as our degree. We will always cherish the support they gave us and for always being there to listen to our rants.

About 8 months ago, 3 ambitious about-to-be young engineers selected this topic for their Final Year Project, dazed by the challenge it presented. The next 8 months exceeded their expectations; it challenged their patience, drive, motivation, engineering skills, friendship… and sometimes even their sanity. Looking back on these 8 months, it was the right challenge that these young engineers needed before graduation. In conclusion, we would like to acknowledge ourselves for putting up with each other. This project helped us to become better individuals, engineers, team members as well as friends. The lessons we take away from this project and this experience are invaluable, and we most certainly would not change any aspect about what this project was, under whose supervision it was executed and most importantly, the team members that worked on it.

ORIGINALITY REPORT

FYP Report V2

ORIGINALITY REPORT

13%	12%	4%	4%
SIMILARITY INDEX	INTERNET SOURCES	PUBLICATIONS	STUDENT PAPERS

PRIMARY SOURCES

1	hdl.handle.net Internet Source	4%
2	scitechdaily.com Internet Source	3%
3	www.sunspiral.org Internet Source	2%
4	Julian J. Rimoli. "On the impact tolerance of tensegrity-based planetary landers", 57th AIAA/ASCE/AHS/ASC Structures, Structural Dynamics, and Materials Conference, 2016 Publication	1%
5	mafiadoc.com Internet Source	1%
6	ccsl.mae.cornell.edu Internet Source	1%
7	mars8.jpl.nasa.gov Internet Source	<1%
8	www.mae.cornell.edu Internet Source	<1%

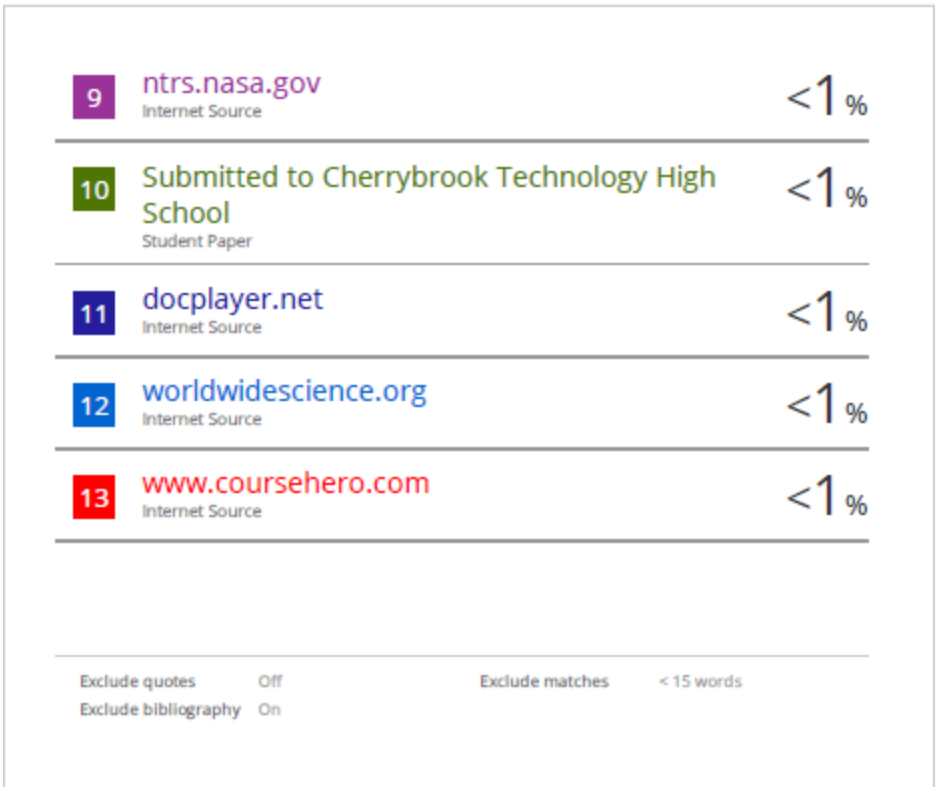
9 ntrs.nasa.gov
Internet Source
<1%
10 Submitted to Cherrybrook Technology High School
Student Paper
<1%
11 docplayer.net
Internet Source
<1%
12 worldwidescience.org
Internet Source
<1%
13 www.coursehero.com
Internet Source
<1%
Exclude quotes Off
Exclude bibliography On
Exclude matches < 15 words

TABLE OF CONTENTS

LIST OF TABLES

TABLE OF FIGURES

ABBREVIATIONS

CSV	Comma-Value-Separated
DOF	Degree of Freedom
DTRL	Dynamic Tensegrity Robotics Lab
ERM	Eccentric Rotating Mass
EDL	Entry, Descent & Landing
FEA	Finite Element Analysis
FOS	Factor of Safety
MSL	Mars Science Lab
NIAC	NASA Innovative Advanced Concepts
NTRT	NASA Tensegrity Robotics Toolkit

CHAPTER 1: INTRODUCTION

The aim of this final year project is to design a dynamic tensegrity structure that is capable of operating on a planet other than earth or a terrestrial satellite, in course of a space mission. The target terrestrial satellite for the course of this project was Titan, Saturn's largest Moon.

Motivation

A complex engineering problem of this nature is the right challenge for a Final Year Project. The project would enable the group to go through the entire product development stages. This project pushed the group to explore years of research done on tensegrity structures and its applications in NASA's newest space probe concept as well as decades of research into space exploration which was exactly the kind of exponential enhancement that was needed in the learning curve for senior engineering students.

Objectives

The objectives of the project were:

1. Proposition of a configuration for the Tensegrity Robot
2. Modelling of Tensegrity Robot
3. Perform structural analysis on the Tensegrity Robot
4. Propose a control system that can make the structure dynamic

The project's primary objective was essentially to demonstrate and validate the tensegrity robot as a capable Entry, Descent, Landing (EDL) system and primary equipment for mobility. Using a tensegrity structure in this way allows the tensegrity probe to make up a greater proportion of the entry mass than other missions like Pathfinder, the Mars Exploration Rover missions, or the Mars Science Laboratory (MSL) project.

Tensegrity Structures

Tensegrity, a portmanteau of tensional integrity, is a structure that uses discontinuous compressive elements (struts) linked to a continuous network of tensile elements (cables) to maintain a stable volume in space [2]. Examples of tensegrity structures are shown in Figure 1.

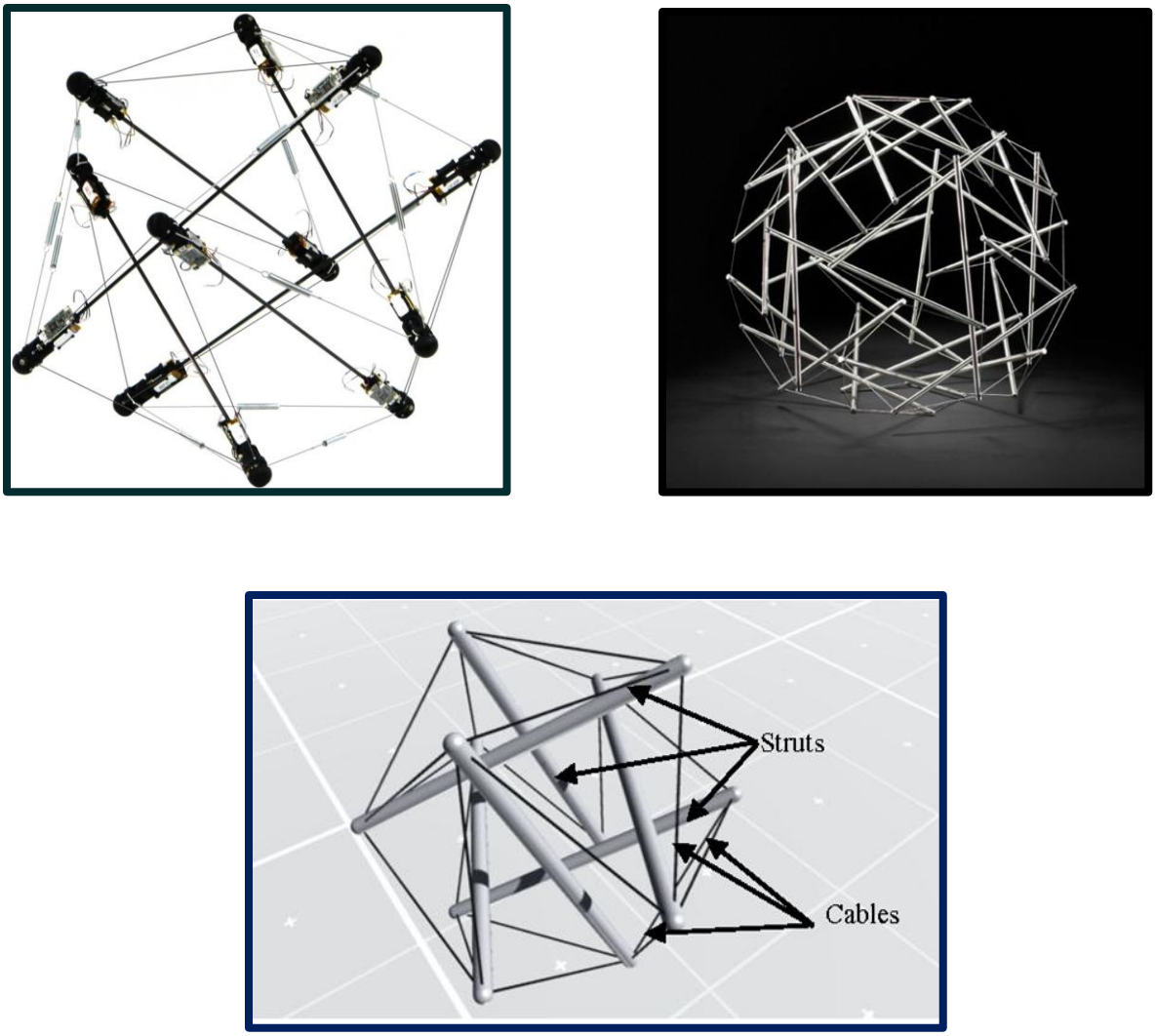

Figure 1: Examples of Tensegrity Structures [35] [36] [37]

Tensegrity and Space Exploration

Research in Tensegrity robots is of interest due to the low-cost alternative they provide in planetary exploration missions. There are a few reasons tensegrity structures manage to do so:

1. Several tensegrity robots can fit into a small launch platform.
2. After they initially enter the atmosphere and the heat shield is ejected, they can automatically be moved away from each other in order to land at their destination.
3. They possess the ability to bounce upon impact. This means that no equipment is needed to reduce their final descent speed.
4. Upon landing, they are fully capable of re-orienting themselves, without the help of additional hardware, and begin performing measurements through attached sensors.
5. They allow a more aggressive approach to exploration since they are capable of surviving significant falls and are not prone to being stuck which brings about ease of route planning.

Benefits of Tensegrity Structures

There are quite a few features that give an edge to tensegrity structures over other structure types. The features are discussed below:

Reusability

The modular rods, which are under compression, do not need to be custom fit for different missions. The same rods can be reused in different configurations for future missions.

Redundancy

They function as independent entities which means that they can be used as landing and mobility platforms, both at once, without using additional hardware.

Reliability

Several robots can be packed tightly together for transit, which increases the coverage during missions and lowers the risk of failure allowing significantly faster scientific return. The structures are reliable because even upon several actuator failures, they stay robust to a complete loss in range of motion, only experiencing a gradual performance degradation. Additionally, they have a high tolerance to impact loads, which means that they can be used without the need to slow down their descent speed.

Reduced Mass and Cost

Science payload ratio is the percentage of the total weight that is used to accomplish space missions. The higher the payload ratio, the more cost effective the solution, which so far has been highest for tensegrity while considering mobile platforms. A comparison of mass of various types of structures is given in Table 1.

Table 1: Comparison of Rovers available for Space Missions

	Pathfinder	**MER**	**MSL**	**Huygens**	**Tensegrity**
Mass at Entry (kg)	587.00	831.00	3301.00	320.00	140.00
Mass at Landing (kg)	372.00	540.00	943.00	223.00	100.00
Mass of Rover (kg)	11.00	175.00	943.00	0.00	100.00
Science Payload and Support Avionics (kg)	8.00	146.00	723.00	223.00	70.00
Productive Science Mass Percentage	1%	17%	22%	69.7% (No Mobility)	50%

Tensegrity Mission Specifications

With current space probes lacking the capability to function on various unexpected terrains, the need for small, lightweight and low-cost missions has become increasingly important for advanced space exploration. Tensegrity structures are highly compatible in this regard; with ideal teams of small and collapsible robots being launched and unpacked separately at specific destinations, rapid and reliable on-site exploration is possible.

The NASA Ames Research Centre, with its Dynamic Tensegrity Robotics Lab (DTRL) has been focused on the development of compliant and reusable tensegrity robotic platforms for planetary missions. Work up till now includes the SUPERball; a spherical, underactuated exploratory robot made up of a matrix of cables and joints that could survive being dropped from a spacecraft high above a planet's surface and bounce back.

Once the robot lands on the surface of the planet, the control system can actuate the structure to move in any direction while the central payload collects data with the data acquisition means planted in its core. Due to its ability to absorb and remove energy and its elastic oscillatory nature, the robot can move by rolling in an energy efficient way.
Saturn’s moon, Titan, has a soft surface like a hazardous marsh with large amounts of liquid methane accumulations that would not suit a traditional rover as it would sink down and get stuck. However, the characteristics of the Super Ball Bot; lighter weight and ease of manoeuvrability, allow it to be the perfect substitute for making the exploration mission to Titan a reality.

CHAPTER 2: LITERATURE REVIEW

A literature review was carried out to study and finalise different aspects of the form and use of tensegrity structures and robots. This research is divided into the categories discussed below:

Why Tensegrity over Conventional Rovers?

The ability of tensegrity systems to disperse forces internally is a unique feature. The fact that there are no lever arms, keeps the forces from amplifying across joints or other prevalent points of failure. External forces, on the other hand, are distributed across the framework across multiple load paths, resulting in system-level dependability and resistance to forces from all directions. Resultantly, this allows tensegrity structures to be easily reoriented in gravity fields, making them suitable for use in dynamic environments with unpredictable contact forces. Tensegrities can also withstand the failure of individual actuation elements, resulting in a gradual degradation of overall workspace rather than the complete loss of ranges of motion seen in serial manipulators. [3]

Mission Requirements

The Huygens probe's success shed light on Titan's atmosphere and surface conditions, which were discovered to have elements that were strikingly similar to those found on Earth while also having elements that were starkly different. Factoring in its massive atmosphere, Titan is the largest satellite in the solar system. Titan's dense, icy atmosphere is mostly nitrogen, along with traces of argon, methane and other hydrocarbons. It has been observed to also have a noticeable greenhouse effect, clouds, seasons, traces of a methane-based hydrological cycle, and a highly heterogeneous surface of methane-ethane reservoirs, dune fields, erosion evidence, and suspected cryovolcanism. According to NASA’s work on the Titan Mission, the requirements of the space operation are to be similar to that of the Huygens mission, with the specifications as follows:

- Upon arrival after 8-10 years of transit, the tensegrity probes enter the atmosphere with a carefully calculated approach vector, behind a heat shield which is ejected after sufficient thermal loads have been surpassed.
- The probes then expand into a fully deployed shock absorbing state. For tensegrity structures built with elastic cables, this un-packing can happen automatically.
- Each probe is launched to impact the surface, at Titan's terminal velocity of 11m/s, without requiring parachutes or other landing devices, absorbing and distributing impact stresses while protecting its science payload.
- The equipment that is needed to carry out the mission is in three packages, as follows:
    - Package for tracking the atmosphere and meteorology
    - Package for analysing the surface and atmospheric chemistry
    - Package for Imaging Equipment

      This equipment was also used to estimate the initial requirement of avionics power and the structural support for a safe mission.

The analytical chemistry kit will analyse the organic molecules on the surface in great detail. Complex organic chemistry on Titan's surface that can produce and maintain organic molecules may provide insight into prebiotic chemistries in the solar system.
As the tensegrity robot moves over Titan's surface, an atmospheric and meteorology instrument kit can continuously track temperature, pressure, wind speed, and methane humidity. At many locations around the surface, the atmospheric and meteorology kit can calculate diurnal and probably seasonal changes in temperature, wind speed and direction, and methane humidity variations, enabling the detection and monitoring of local weather systems. A NAVcam and a field microscope will be included in the imaging kit, which will be used in a number of surface operations. The tensegrity robot NAVcam will be similar to the NAVcams used by the Mars

Exploration Rover (MER), but with larger heating elements to cope with Titan's harsh climate. It will be used to traverse the varied terrain. [4]

Tensegrity Rover Configurations

Two main configurations of tensegrity rovers are available in literature: a spherical ball and a tetraspine structure.

A modular tensegrity robot inspired by the spine with robust robotic locomotion was developed, initially, to better understand how vertebrates coordinate motion with a compliant spine. It was named the Tetraspine and as shown in Figure 2 and 3, it was built using rigid tetrahedron-shaped segments connected by six cables amongst them. This method was opted for in order to eliminate rigid joints between segments and increase the compliance in the structure. The structure was robust to disturbances and traversed multiple types of irregular terrains successfully in simulation. Using prototype hardware, the viability of the overall structure for locomotion has been proved. [5].

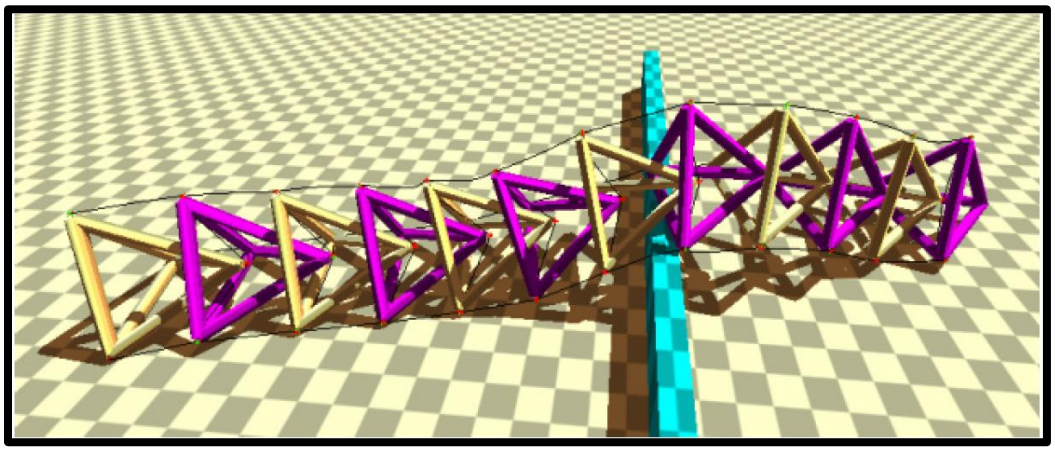

Figure 2: A tetraspine tensegrity structure [5]

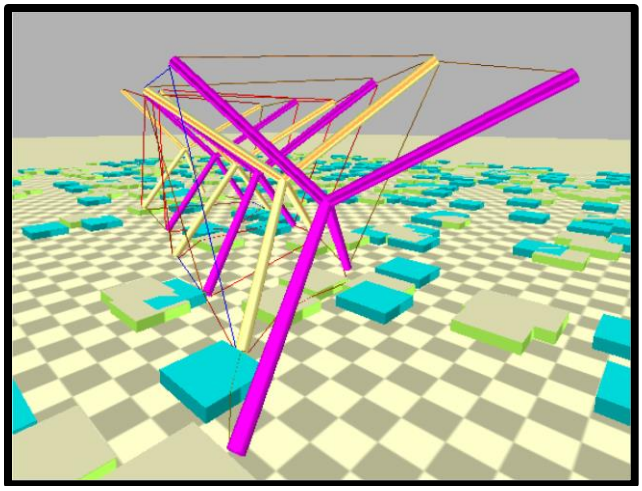

Figure 3: Another tetraspine tensegrity structure

On the other hand, the spherical configuration, shown in Figure 4, consists of compression elements, axially loaded and positioned within a network of tensional elements. Hence, they only experience either pure tension or pure linear compression. As a result, the individual compressional elements can be very lightweight since they are not put under any bending or shear forces. These can be packed together in small launch volumes to be deployed whenever needed. [4]

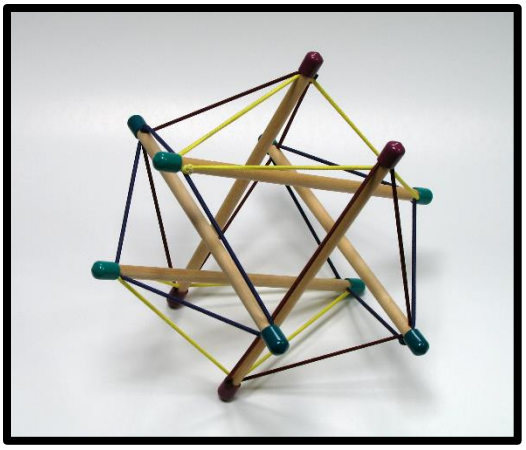

Figure 4: A Spherical Configuration - Icosahedron [38]

From studied literature, it is evident that both structures are generally robust to perturbations and do operate in several types of irregular terrains successfully in simulation. However, research so far shows that the spherical configuration can be controlled using multiple control systems such as morphological computation, cable colocation and more whereas the Tetra Spine structures use distributed impedance controllers along with central pattern generators (CPGs) that generate tuneable motion in the structure. In addition, the spherical configuration is comparatively more robust to actuator failure than the tetra-spine structure making it a lot more resistive to complete failure in comparison to the Tetra Spine structure.

Therefore, a spherical configuration was selected for this project.

Within the spherical configuration, so far, the 6, 12 and 30 strut morphologies, shown in Figure 5, 6 and 7, are possible:

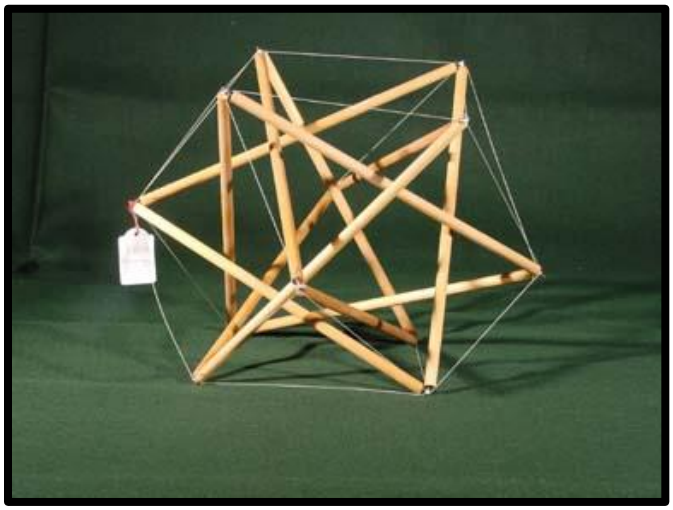

Figure 5: A 12 strut tensegrity structure [39]

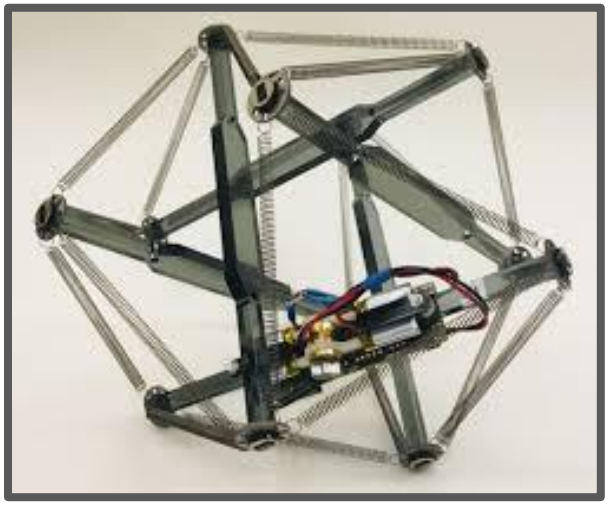

Figure 6: A 6 strut Tensegrity structure [34]

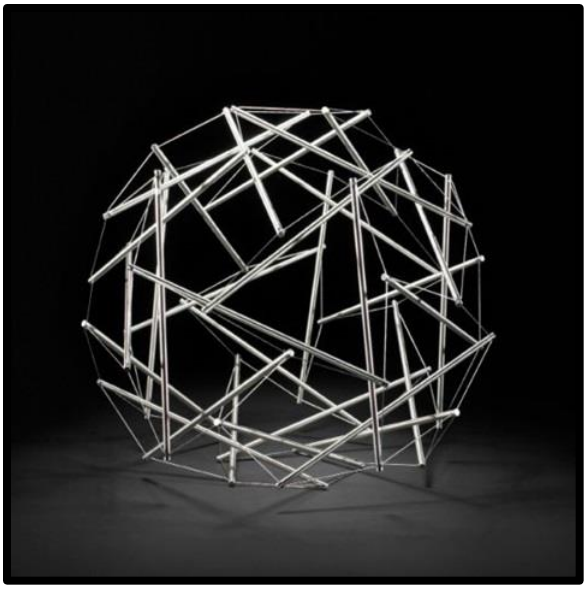

Figure 7: A 30 strut Tensegrity structure [36]

Smaller morphologies can also be opted; however, they are unable to imitate the spherical shape properly which leads to problems in locomotion with any selected locomotion system.

Comparing the options, the 6-strut morphology holds great benefits over the other two configurations in terms of final weight and size of the structure. Thus, more 6 strut robots can be packed together in transit compared to structures in the 12 and 30 strut configurations. In conclusion, it would be easier to integrate more struts into a configuration once an initial 6 strut system has successfully been designed and analysed and that is why the finalized configuration is of the 6-strut spherical robot.

Strut and Cable Specifications

Impact simulations at different velocities ranging from 10m/s to 18m/s, conducted by NASA, for the SuperBall Bot indicated that the deceleration of the scientific payload with airbags is matched and bettered by a strut length of 8 m.

However, the existing aeroshells in use, which act as heat shields in the initial descent of the rovers, have a diameter of 4.5 meters, just like the one used in NASA's Curiosity rover to Mars. Thus, this limits the maximum strut length that can be covered by it, up to 3.8 meters. The robots with 3.8-meter struts can then be packed in the star elongation shape, which is discussed further in the report, for mission deployment.

For cables, the tensional elements of the system, the spring constant and the pre-tension play a vital role in the strength of the structure along with the methods of collapse and expansion. With simulation-based experimentation, it was discovered that a higher spring constant meant that the structure would not collapse easily on impact and stays rigid, resulting in high deceleration of the scientific payload. Whereas, a lower spring constant, can result in the structure being completely compressed, resulting in the payload hitting the ground as well. Furthermore, a higher pretension results in higher stresses in struts and more resistance to locomotion and in contrast, a lower pre-tension results in high tension in the cables.

Methods of Collapsing and Expanding

Based on the survey of existing bots, two primary ways of collapse and expansion were identified; the star elongation and linearly extended methods as discussed below.

1. Star Elongation

In this method, the actuated faces are oriented at the top and bottom of the structure, with the cable faces elongated to collapse the whole structure. The height of the structure here depends on the tensional elements used. This method is preferable in terms of storage, as it allows the most effective use of the space available. Following figures show the beginning and final stages of this method.

Figure 8: Collapsing into the star elongation shape. [3]

2. Linearly Extended

In this method, the actuated faces are oriented at the right and left of the structure, with the cable spooling in the cylindrical strut and collapsing the structure linearly.

Figure 9: Structure collapsing into linearly extended shape. [3]

Structural Analysis of Tensegrity Robots

For the structural analysis of tensegrity systems, we looked into NASA's cerebration of the characteristics required by the structure to withstand all landing orientations at a height that corresponded to the impact velocity on Titan which is 11 m/s. This matched the velocity attained by a 10-meter fall here, on Earth. They were successful in this feat, and the structure demonstrated the tensile strength of the tensegrity principles after a 10-meter fall. Even when the tensegrity lander's overall structure was put to the test and several attachment points failed (as expected), the overall structure remained intact.

The NASA Tensegrity Robotics Toolkit (NTRT), the team's primary simulation environment, is based on the discrete time Bullet Dynamics engine (a game physics simulator) [22]. NTRT's main benefit is that it allows researchers to study how tensegrity robots communicate and travel around virtual environments. This has made prototyping and simulating the robot easier, which reduces the amount of CAD work required. The NTRT is a resource that has been made open source. In the Linux-environment, it is available on GitHub.

The Euler-Lagrange simulator, which was also used, predicts payload acceleration during drop tests, stiffness assessments, and form-finding. Its simplistic underlying model, on the other hand, makes it unsuitable for studying complex interactions with the environment. As a result, it is only suitable for studying particular limited circumstances and cannot accommodate rich and complex environmental interaction. NTRT allows for the development of various terrains and obstacles, as well as the control of tensegrity robots across those terrains using active sensor feedback.

Since game physics necessitate real-time simulation, Bullet is devised to handle collisions without using too much computing power. However, the Bullet physics library currently lacks practical material properties and stress analysis models for chains, wires, and springs. Instead, the NIAC team created an additional library to simulate spring-cable assemblies as two-point tensional

elements that introduce directional forces to rigid bodies instead of using the default soft body models.

Using more mathematically rigorous models, this approach allowed for the calculation of the corresponding stretch and tension for each simulated cable, as well as the force applied to the bodies. They had a drawback with this approach at first: the cables did not exist as real bodies in the simulation environment, so their collisions and interactions with rigid bodies were not simulated. This limitation was irrelevant for much of their research since they were researching locomotion on relatively flat terrain. They recently introduced a cost-effective method for using soft body touch dynamics in the elastic cables. As a result, they assume NTRT is one of the few open-source libraries with an effective and practical model of elastic cable dynamics. With this new capability, they were able to begin studying locomotion over more complex terrain, where the cables are expected to come into contact with and communicate with the environment as part of the locomotion gait. The NTRT simulator was also cross-validated by other analytic methods and several hardware tests, giving the NIAC team confidence in the simulator's performance. NTRT was also published as an open-source project, and an international group of tensegrity robotics researchers has contributed and used it.

Buckling in Tensegrity Structures

A planetary landing event can be reduced to the dissipation of kinetic energy carried by the vehicle prior to touchdown in structural engineering terms. Structural damping, friction between the structure and the ground, and probably aerodynamic drag are all common dissipation mechanisms. In the worst-case scenario, the vehicle's entire kinetic energy is transferred to its structure during the first collision. If permanent harm is to be avoided, the lander's structure must store all of the kinetic energy as elastic strain energy, which can then be dissipated using the aforementioned mechanisms.

According to Julian J.Rimoli of Georgia Institute of Technology, the assumption that a tensegrity system will collapse due to buckling and yielding loads, under high dynamic impact loads, such as in landing events, is invalid. The bar members could experience major deformations, and the existence of body forces would mean that both bars and cables will suffer off-axis loads. In his research (Figure 10), under highly dynamic events, buckling of individual members of a tensegrity system does not inherently mean structural collapse, as shown by a reduced-order model capable of capturing their buckling and post-buckling activity. His research suggests that allowing planetary landers' compression members to buckle may result in more efficient structural design. [6]

In the previously used Entry, Descent and Landing (EDL) systems as employed in the Mars Pathfinder, airbags were used to cushion the spacecraft in the case it lands on rocks or rough terrain and allowed it to bounce across Mars' surface at small speeds after landing. To add to the

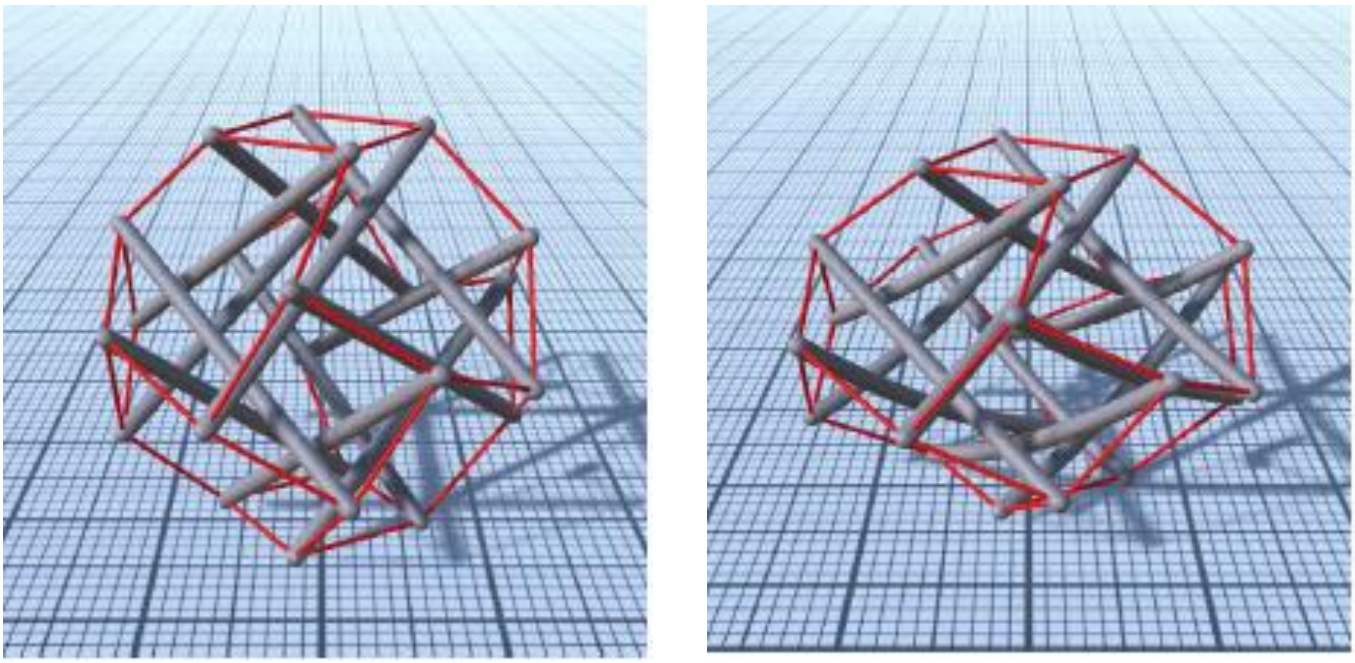

Figure 10: The structure collapsing on impact [6]

complexity, the airbags were to be inflated seconds before touchdown and deflated once safely on the ground. [7]

But with the tensegrity platform, the risk of airbag deployment failure is eliminated, along with a reduction of the weight it adds to the system which is the prime initial cause of abrasions and tears. Instead, the deployed tensegrity struts compress on impact, with the cables absorbing the energy of impact, as shown in the figure 11:

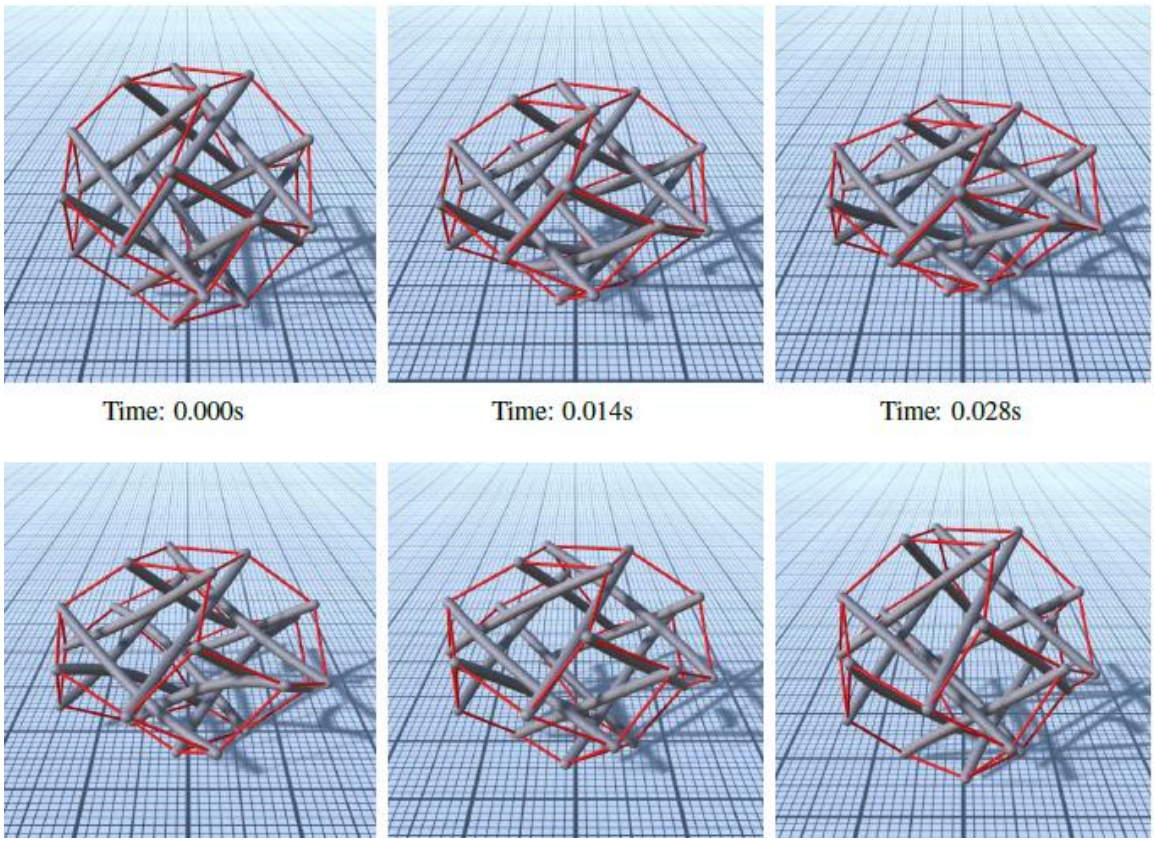

Figure 11: The structure restores its original shape after impact [6]
Temporal evolution of a virtual drop test for a tensegrity lander with impact velocity v = 6m/s

Overall, these properties enable tensegrity structures to uniformly distribute strain energy throughout the entire system, withstand severe deformation, and finally recover its original form. And with the proper exploitation of the post-buckling responses by tensegrity structures, we can develop highly efficient lightweight tensegrity landers.

Control System

The control system for tensegrity structures can be divided into 2 main parts: the control architecture and the actuation system.

A common trend across the literature, for the control architecture, is the use of Genetic/Evolutionary algorithms [8] [9] [10], Central Pattern Generators [11] [12] [13] and bootstrap algorithm [14] to control the actuation system. This prevents the need for the complex, non-linear physics of dynamics to be modelled [3] [4] [15]. Therefore, the objective for the control system design was to realize an open loop actuation system.

The choice of actuation (locomotion) systems can be generally divided into 4 categories [16]:

1. Strut Collocated
2. Cable Collocated
3. Non-Collocated
4. Morphological Computation

The first 3 choices of locomotion systems share a common aspect, they manipulate the shape of the tensegrity structure. This allows for the line of action of gravity to pass outside of the base, which helps to roll the structure over. Repeated manipulation of the shape allows for a continuous rolling gait.

Strut Collocated

In strut colocated actuation, the actuators are responsible for altering the strut lengths [17], and as a result the overall geometry of the structure.

Cable Collocated

In cable colocated actuation, the structure is modified by changing the effective rest length of the cables. [16]

Cable collocated actuation can be achieved by several means:

1. Electrical Actuators [16] [18] [19]
   In Electrical Actuators, motors are used to change the rest length of the cables.
2. Pneumatic Actuators [20]
   Pneumatic Actuators, e.g., McKibben Actuators, are also known as Pneumatic Artificial

Figure 12: McKibben Actuators in their rest state and under pressure (left to right) [32]

Muscles. These actuators are used in place of the cables and have the capability of changing their length under increased internal pressure.

3. Light Based Actuators

   Light Based Actuators are a novel way of controlling the rest length of the tensile element (cable). Similar to Pneumatic actuators, the actuators form the tensile element themselves. Zhijian Wang et al. worked on using Liquid Crystal Elastomer - Carbon nanotube composites as the artificial muscles whose length can be changed by the application of light. [21]

4. Shape Memory Alloys [22]

   Shape Memory Alloys are alloys that deform when cold, but return to original shape when heated. Similar to Light Based Actuators and Pneumatic actuators, SMAs are used as the tensile element and with temperature being used to control their rest length.

Non-Collocated

Actuation is applied between two struts, two cables, or a strut and a cable in non-colocated actuation.

Morphological Computation [14] [15]

Morphological computation is a system that takes its inspiration from the natural world. Morphological computation argues that the body should outsource at least some forms of regulation (such as walking or grasping) because these functions are already “encoded” within it. Another way of looking at it is that the human body can be used as a computing resource. This simplifies a task by reducing the sophistication of the robot's computational problems and the associated control and learning tasks, since part of the "work" has already been performed by the body. This idea helps the human/animal body to perform tasks such as walking and other activities with minimal brain intervention.

The use of vibration in tensegrity structures allows for morphological computation. Vibrating Motors attached to the strut vibrate at one of the system's natural frequencies, allowing the structure to move.

Unlike its sister locomotion systems, morphological computation is special. Instead of rolling, it develops a walking-like gait. Furthermore, the vibrational frequency mixture to be used has no analytical solution and must be discovered by experimentation [15]. In comparison to other locomotion systems, morphological computation has a distinct advantage in that it needs the least amount of computing power to achieve better locomotion speeds. In a comparative analysis drawn by Mark et al. the tensegrity robot using morphological computation achieved faster locomotion with a much simpler locomotion system compared to previously researched experimental tensegrity models that used collocation-based locomotion systems [15].

Materials

The materials used in space are always the most sophisticated materials ever devised by humans, and there are active studies and developments for new and better materials. To be efficient in space, these materials must have a number of specific properties. Explicitly for Titan, which has surface temperatures around −179 °C, and down to −202 °C at higher altitudes [23], we require a space grade material capable of withstanding high impact stresses at cryogenic temperatures, with low density to ensure a higher science payload ratio.

For general space applications Kevlar, Aluminium and Titanium are the prime candidates. Kevlar, a lightweight and robust material commonly used in protective vests and armour, is ideal for space flight. Aluminium is another lightweight material that is often used in space. Aluminium is not very strong on its own, but it becomes much better when mixed with other metals to form alloys. The alloys that are created are generally strong and light enough to be used in space structures and satellites [24]. The shutters on the windows of the International Space Station are made of aluminium to shield them from impacts. [25]

And where lighter aluminium alloys no longer meet strength, corrosion resistance, or elevated temperature specifications, titanium alloys are used as can be seen in Figure 13. [25]

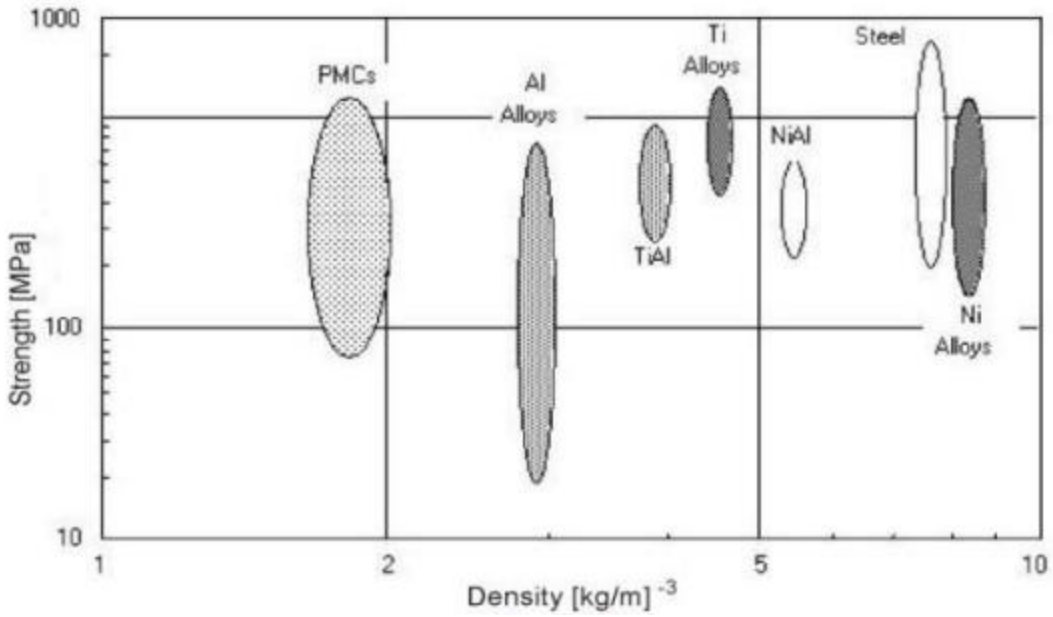

Figure 13: Space Grade Material Properties [25]

According to the resources available, it can be seen that aluminium alloys are used at both room temperature and in cryogenic applications, with research focusing on further reducing the density, improving the elevated temperature capabilities and the corrosion resistance of these alloys [26]. And after a thorough examination of various material properties, the best option was determined to be 6061 T6 Aluminium Alloy for the struts of our tensegrity robot.

Previously used EDL Specifications [7]

To mitigate impact forces and position a robot in the correct orientation, current robot designs are fragile, requiring a complex combination of devices such as parachutes, retrorockets, and impact balloons. The sequence of events before landing is explained below:

Final Preparations

Ten minutes before atmospheric entry, the spacecraft sheds its cruise stage, housing radios, solar panels and fuel tanks used on the journey to Mars. Only the protective aeroshell, which contains the rover and the descent point, makes the journey to the surface. Small thrusters situated on the backshell are fired before entering the atmosphere to ensure that the heat shield is facing forward for what follows.

Atmospheric Entry

The drag created as the spacecraft enters the Martian atmosphere significantly slows it down – but these forces also dramatically heat it up. The heat shield external surface temperature reaches to about 2,370 degrees Fahrenheit around 80 seconds after atmospheric entry, indicating peak heating (about 1,300 degrees Celsius). When the spacecraft continues to descend through the atmosphere, it encounters pockets of air that are more or less thick, which can cause it to deviate from its intended route. It adjusts its angle and direction of lift by firing small thrusters on its backshell to compensate. This technique of "guided entry" aids the spacecraft in staying on course for its downrange target.

Parachute Deployment

The spacecraft is slowed to less than 1,000 miles per hour by the heat shield (1,600 kilometres per hour). It's safe to deploy the supersonic parachute at this stage. Perseverance uses a new technology called Range Trigger to measure the distance from the landing target and open the parachute at

just the right moment to reach its target. At an altitude of about 7.00 miles (11.00 kilometres) and a velocity of about 940.00 mph, the parachute, which is 70.50 feet (21.50 metres) in diameter, deploys about 240.00 seconds after entry (1,512.00 kph).

Zero In on Landing

The heat shield separates and falls away 20 seconds after parachute deployment. For the first time, the rover is exposed to Mars' atmosphere, and main cameras and instruments will begin to lock onto the rapidly approaching surface below. Its landing radar bounces surface signals to determine its altitude. Meanwhile, Terrain-Relative Navigation, a new EDL technology, kicks in. The rover uses a special camera to easily locate features on the surface, which it compares to an onboard map to determine its exact location. Members of the mission team have plotted out the best areas of the landing zone ahead of time. If Perseverance detects that it is approaching more dangerous terrain, it chooses the safest spot available and prepares for the next dramatic move.

Powered Descent

The parachute will only slow the vehicle down to around 200 miles per hour in the thin Martian atmosphere (320 kilometres per hour). Perseverance must break itself out of the parachute and use rockets to get to its safe touchdown speed. The rocket-powered descent stage is located directly above the rover, within the backshell. Consider it a jetpack with eight engines aimed at the ground. The rover separates from the backshell and fires up the descent stage engines once it's about 6,900 feet (2,100 meters) above the earth.

To avoid being impacted by the parachute and backshell coming down behind it, the descent stage easily diverts to one side or the other. The safe target chosen by the machine that runs Terrain-Relative Navigation determines the course of its divert manoeuvre.

Skycrane Manoeuvre

As the descent stage levels out and slows to about 1.7 miles per hour, the "skycrane" manoeuvre begins (2.7 kilometres per hour). The descent stage lowers the rover on a series of cables about 21 feet (6.4 meters) long about 12 seconds before touchdown, at about 66 feet (20 meters) above the surface. Meanwhile, the rover's mobility mechanism is untucked, and its legs and wheels are locked into the landing place. When the rover detects that its wheels have made contact with the earth, it quickly disconnects the cables that link it to the descent point. This allows the descent stage to fly away and land on the surface in an uncontrolled manner, safely away from Perseverance. [7]

Initial Design Specifications

From the studied literature, an initial design proposition was made. Geometrically, the structure configuration would be that of a 6-strut ball bot with each individual strut length 3.8 metres in length. The material for the struts was chosen to be 6061-T6 Aluminium alloy whereas, for the cables, 1080 Spring Steel was selected. Furthermore, to completely define the initial design specifications of the structure, Morphological Computation was chosen as the actuation system to be incorporated in the structure.

CHAPTER 3: METHODOLOGY

The methodology adopted for this project has been first studying the available configurations of structures that can be deployed on rough to marshy terrains, developing an understanding of our design specifications to create an initial design and finalizing it, followed by the CAD Model development in order to perform eigen value and finite element analysis for the development of a stable system. The last is the control system implementation to validate the complete system. Figure 14 summarizes our approach:

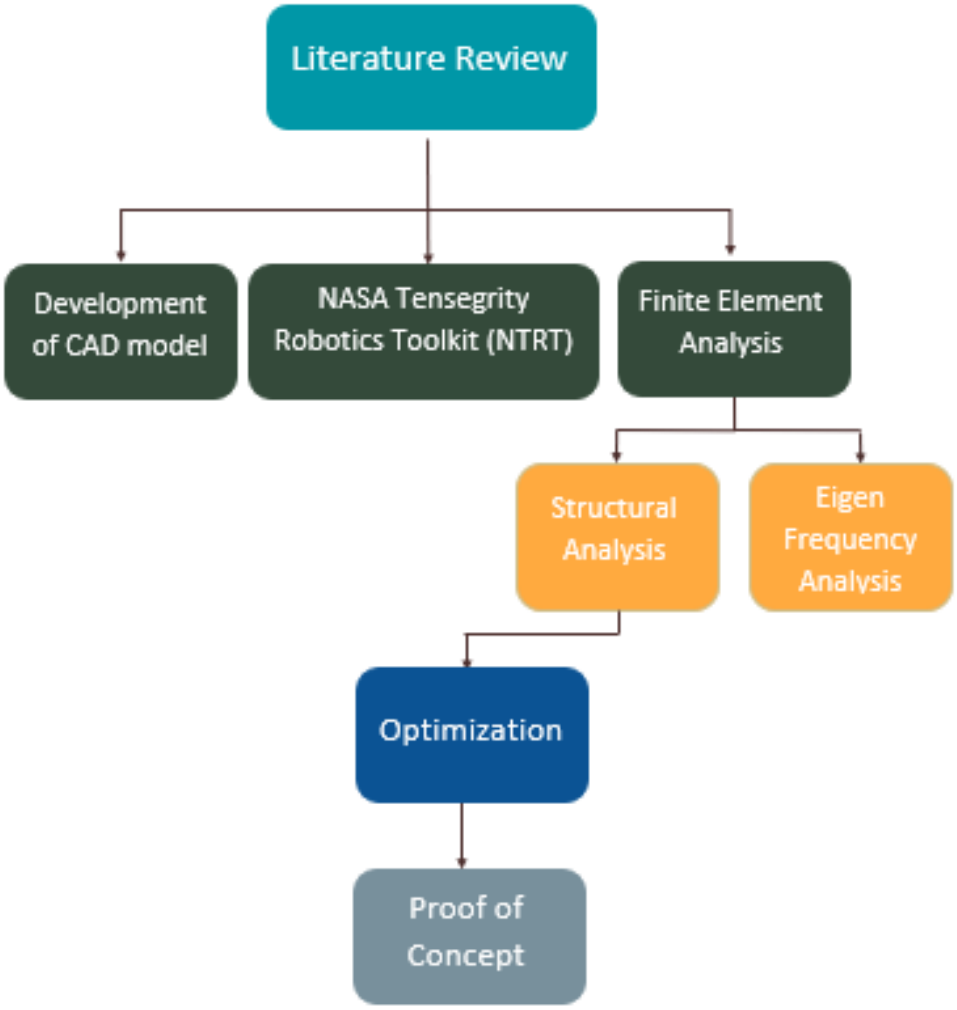

Figure 14: A flowchart of the methodology

Computer Aided Design

It was decided to design the structure using Solidworks.The design consists of two hollow rods in each plane with ends coincident to each other when in the neutral position. The rods were made by using the Cut Extrude tool through an already extruded cylinder. Four slots were made in the struts at each end for the cables to go through. The cables were added to the assembly as a part within the assembly and constrained to stay within their slots at each end. Using the 3D Sketch feature and keeping the cables as separate parts within the assembly, they successfully behaved as tensional members when the compression members (struts) moved from their neutral position for locomotion without getting detached from them.

For the strut-to-cable connection, we decided to design a box that would have a sleeve that goes on each end of all the rods. The box has a slot on each of its faces, where the cable would enter and go around a small pulley making sure all the cables are always in tension throughout impact and locomotion.

For our chosen control system, we had to attach an eccentric vibrating mass motor to each of the struts. We decided to do so by putting a clamp around the centre of each of the struts which could be tightened from two points across the diameter of the clamp. We designed the clamp in such a way that it included a bed for the motor to rest upon and be bolted into so it is able to transfer vibrations with minimal loss in frequency. Finally, the motor was modelled and bolted on top of the clamped bed on each of the six struts.

NASA Tensegrity Robotics Toolkit (NTRT)

NTRT is a collection of open-source C++ and MATLAB software modules that are used to model the structure and control system of Tensegrity Robots. NTRT is based on the Bullet Physics Engine (a game physics simulator) to simulate soft body dynamics and collisions without needing excessive processing power. NTRT is more accurate than commercial Finite Element Analysis

(FEA) softwares for simulating Tensegrity Robots because of the relatively poor representation of soft bodies dynamics in the commercial FEA softwares.

In NTRT the structure is hard coded using the library of modules. The environment's specifications (e.g. magnitude of gravitational acceleration) are coded in C++, the file's code is part of Appendix I: NTRT Code.

The structure itself is coded in YAML language (a markup language). The geometric coordinates of the strut ends, from the Solidworks model, were used as an input in the YAML file. We identified the struts' endpoints, or nodes, as well as whether a strut or cable exists between two nodes. Other model properties, such as rod density and radius, are described below the node coordinates. The default unit of length in the configuration is decimetre, and all subsequent units are derived from it. The density of 6061-T6 aluminium, for example, is 2700 kilograms per meter, or 2.7 kilograms per decimetre, as shown in the rod 'class' at the bottom of the YAML file below:

```
nodes:
  # lines starting like this represent the comments.
  # left vertical rod
  # 2as = v^2, where a = 13.5, v = 120 dm/s; to calculate the height that the structure should drop from
  left_vert_bottom: [-9.5, 532.5, 0]
  left_vert_top: [-9.5, 570.5, 0]

  # right vertical rod
  right_vert_bottom: [9.5, 532.5, 0]
```

right_vert_top: [9.5, 570.5, 0]

bottom horizontal rod

bottom_horiz_prox: [0, 542, -19]

bottom_horiz_dist: [0, 542, 19]

top horizontal rod

top_horiz_prox: [0, 561, -19]

top_horiz_dist: [0, 561, 19]

proxal horizontal rod

prox_horiz_left: [-19, 551.5, -9.5]

prox_horiz_right: [19, 551.5, -9.5]

distal horizontal rod

dist_horiz_left: [-19, 551.5, 9.5]

dist_horiz_right: [19, 551.5, 9.5]

#payload: [0, 19, 0]

payload_top: [0, 20, 0]

payload_bottom: [0, 18, 0]

```
pair_groups:
  superball_rod:
    # coronal plane
    - [left_vert_bottom,left_vert_top]
    - [right_vert_bottom,right_vert_top]
    # sagital plane
    - [bottom_horiz_prox,bottom_horiz_dist]
    - [top_horiz_dist,top_horiz_prox]

    # trasverse plane
    - [dist_horiz_left,dist_horiz_right]
    - [prox_horiz_left,prox_horiz_right]

  actuated_string:
    - [left_vert_bottom,bottom_horiz_prox]
    - [right_vert_bottom,bottom_horiz_prox]

  superball_string:
#   - [left_vert_bottom,bottom_horiz_prox] – as actuated string therefore commented out
    - [left_vert_bottom,bottom_horiz_dist]
    - [left_vert_bottom,dist_horiz_left]
    - [left_vert_bottom,prox_horiz_left]
```

- [left_vert_top,top_horiz_dist]
- [left_vert_top,top_horiz_prox]
- [left_vert_top,dist_horiz_left]
- [left_vert_top,prox_horiz_left]

- [right_vert_bottom,bottom_horiz_prox] – as actuated string therefore commented out
- [right_vert_bottom,bottom_horiz_dist]
- [right_vert_bottom,dist_horiz_right]
- [right_vert_bottom,prox_horiz_right]

- [right_vert_top,top_horiz_prox]
- [right_vert_top,top_horiz_dist]
- [right_vert_top,dist_horiz_right]
- [right_vert_top,prox_horiz_right]

- [bottom_horiz_prox,prox_horiz_left]
- [bottom_horiz_prox,prox_horiz_right]
- [bottom_horiz_dist,dist_horiz_left]
- [bottom_horiz_dist,dist_horiz_right]

- [top_horiz_prox,prox_horiz_left]
- [top_horiz_prox,prox_horiz_right]

```
    - [top_horiz_dist,dist_horiz_left]
    - [top_horiz_dist,dist_horiz_right]

builders:
  superball_rod:
    class: tgRodInfo
    parameters:
      density: 2.7
      radius: 0.15
      friction: 0.99
      roll_friction: 0.01
      restitution: 0.0

  superball_string:
    class: tgBasicActuatorInfo
    parameters:
      stiffness: 22000
      damping: 200.0
      pretension: 8800.0
      history: 0
      max_tension: 100000
      target_velocity: 200000
```

```
  actuated_string:
    class: tgBasicActuatorInfo
    parameters:
      stiffness: 220000
      damping: 200.0
      pretension: 8800.0
      history: 0
      max_tension: 100000
      target_velocity: 200000
```

Finite Element Analysis

Along with using NTRT for simulating the model, Finite Element Method was also used for analysis. A factor of safety (FOS) of 1.5 is normally used in aerospace applications which does not include modelling errors [27], therefore, the target FOS for this project was set to 2.

A tensegrity structure can land at 2 points (Figure 15), the worst-case scenario, or at 3 points (Figure 16), the best-case scenario. The structure was designed for the worst landing case. Additionally, the impact velocity on which to perform the analysis was chosen as 12 m/s, slightly higher than the predicted terminal (and therefore impact) velocity of the tensegrity structure on Titan i.e., 11 m/s.

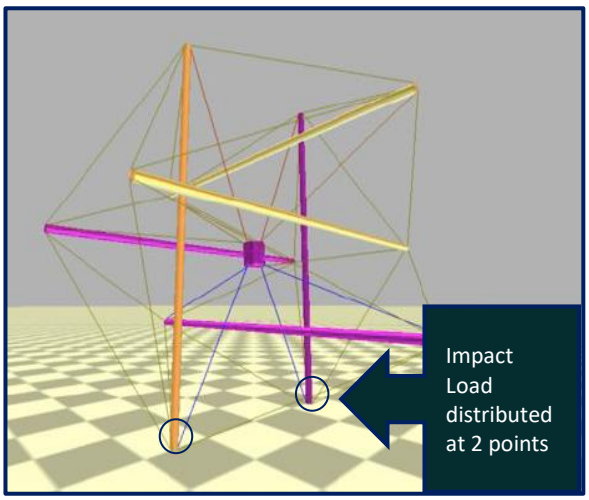

Figure 15: 2 Point Landing [4]

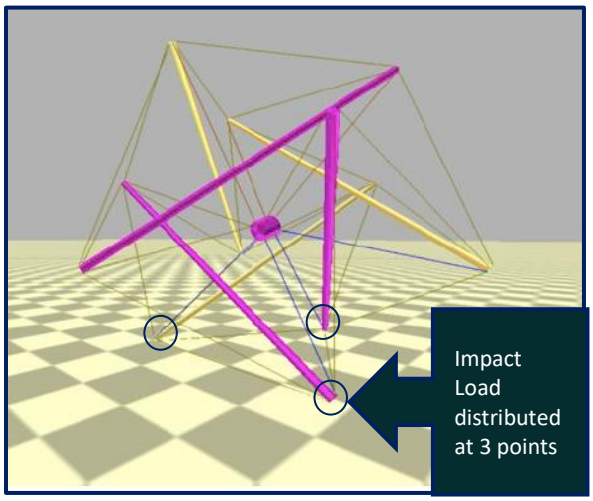

Figure 16: 3 Point Landing [4]

COMSOL was chosen to model the structure in FEA. The geometric coordinates from the Solidworks model were used to model the structure, with all of the elements (both the cables and struts) modelled as Truss. The strut was assigned 6061-T6 Aluminium as its material, whilst the cables was assigned spring steel as its material. The dimensions used were initially the same as those used by NASA in its Phase 2 research [4]. This was done in order to validate the simulation setup.

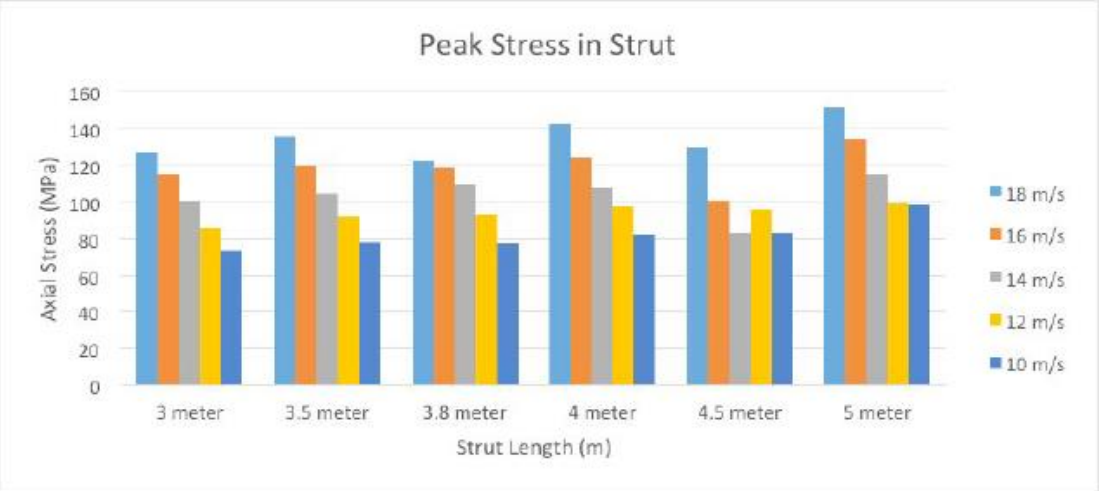

Figure 17: Simulation Results by NASA [4]

The setup was therefore initially designed for a 3.8 m strut length and a strut diameter of 31.75 mm. The structure was analysed in landing configuration with equivalent forces applied on the structure at the points of contact, which were determined using Newton's 2nd Law of Motion:

$$F = \Delta p / \Delta t = m * \Delta v / \Delta t = m * (v_f - v_i)/\Delta t$$

where m = 100 kg (in NASA's case)

$$v_i = 12\ m/s$$

The values of impact force (at each point of contact), final velocity and time duration were found to be:

$$F = 175\ kN$$

$$v_f = 5.5\ m/s$$

$$\Delta t = 0.01\ s$$

The FEA results were validated by comparison with the results available from NASA which are shown in Figure 17.

Eigenfrequency Analysis

The open loop actuation control system requires the natural frequency of the system.

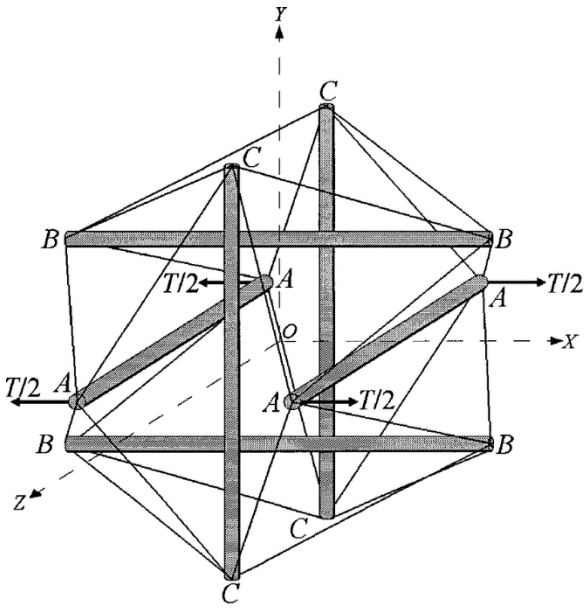

Figure 18: A labelled diagram of a 6-strut tensegrity [33]

As can be seen in Figure 18, each of the strut ends (labelled by letters A, B or C) can move freely even if the other ends are held fixed. Therefore, each strut is a 6 degree of freedom (DOF) sub-system, with the whole tensegrity structure having 36 DOF. This means that the system has 36 natural frequencies.

COMSOL was again used for the Eigenfrequency analysis. Similar to the FEA simulations, the structure was modelled with truss elements, assigning the appropriate materials to the struts and cables.

Optimization

Finalization of the optimal design required the use of component specifications that required the least amount of material, all the while being capable of withstanding peak stresses with a factor of safety of more than 2, an amount higher than the standard 1.5 used in aerospace applications [21].

As the standard aerospace application factor of safety does not include analysis or modelling errors and does not compensate for poor designing or variating material properties, it was believed the factor of safety of 2.0 would cater to the complications in discussion.

Since the initial design started off with NASA's tensegrity strut specifications, the system strut diameter was taken as 3.175 cm. This helped in the cross verification of the resultant stress values upon impact, with NASA's result. Upon verification, the strut diameter was lowered by small values to calculate the impact stresses and the consequent factor of safety. The lowest diameter achieved without compromising on the decided factor of safety was 3 cm which delivered acceptable stresses with a factor of safety of 2.15.

Proof of Concept

A simplified and scalable physical model of the designed structure using paper straws as compression elements and rubber bands as tensional members was developed as a proof of concept, shown in the next Chapter. The success obtained with the proof of concept further solidified the selection for the combination of the design and control system.

CHAPTER 4: RESULTS AND DISCUSSIONS

Computer Aided Design

Figure 19 shows the assembly of the structure in the icosahedron shape, which approaches the ball like configuration. Figure 20 depicts the proposed actuation system will be attached onto the structure with the means of a clamp on the strut. While Figure 21 shows the end box of the strut, into which the cables will go and leave from, continuing onto the next strut's end.

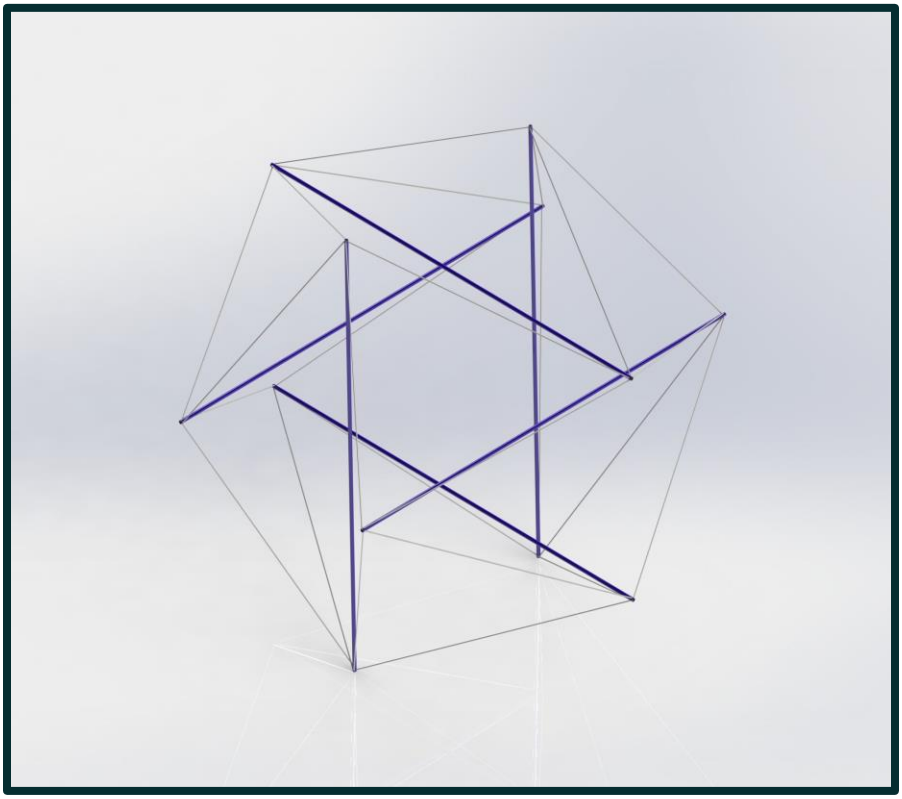

Figure 19: CAD Model of our tensegrity structure

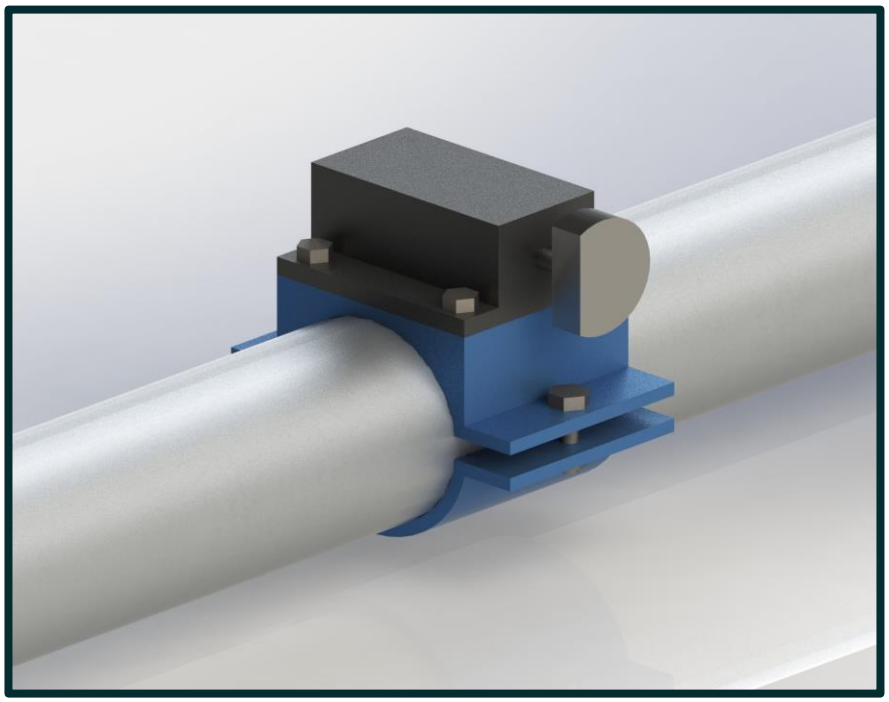

Figure 20: Motor clamped onto the strut

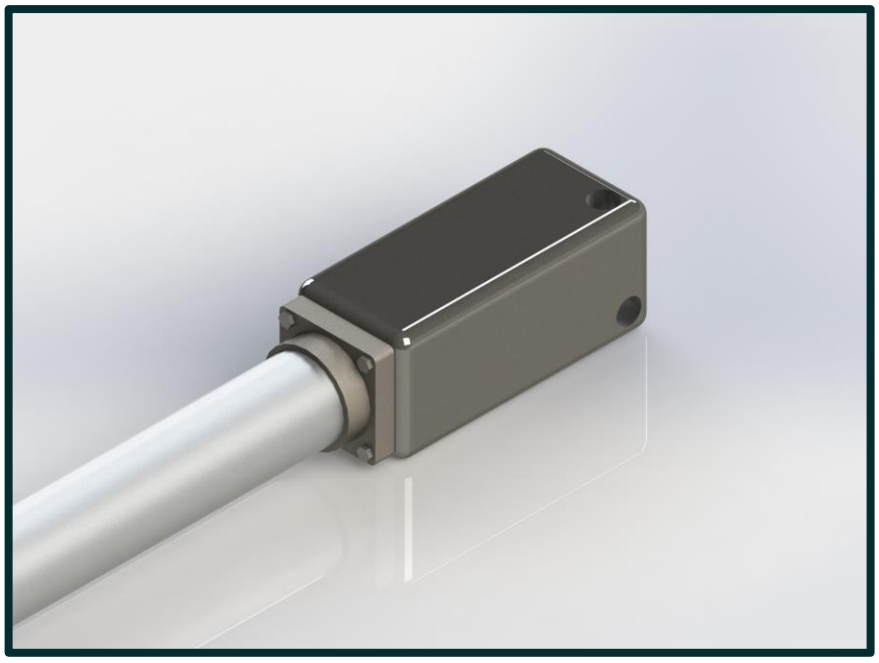

Figure 21: The end of each of strut

NASA's Tensegrity Robotics Toolkit

Performing the simulation on NTRT gave the values of tension in the cables as well as the geometric coordinates of struts with data being logged for a period of 14 seconds around the moment of impact upon landing, at an increment of 0.2 seconds. This data was stored in the form of a comma-separated-value (CSV) File as shown in Figure 22.

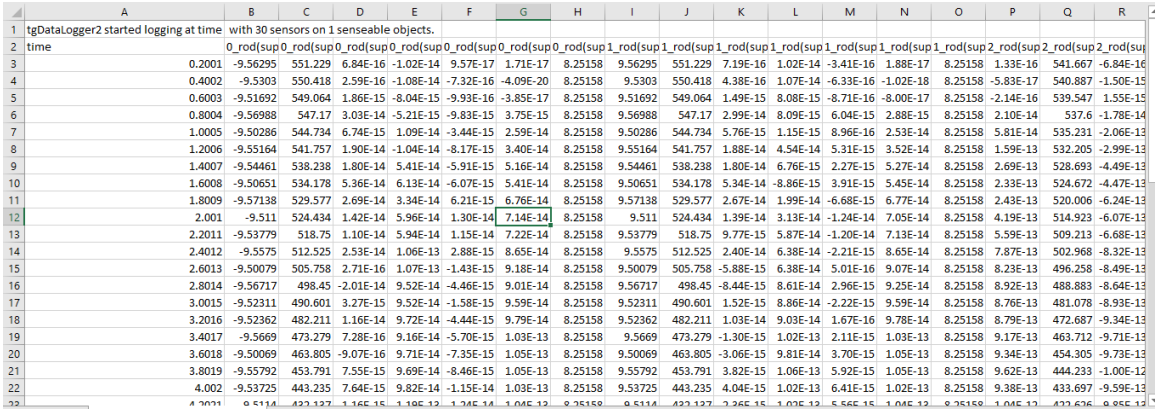

	A	B	C	D	E	F	G	H	I	J	K	L	M	N	O	P	Q	R
1	tgDataLogger2 started logging at time	with 30 sensors on 1 senseable objects.																
2	time	0_rod(sup	0_rod(sup	0_rod(sup	0_rod(sup	0_rod(sup	0_rod(sup	0_rod(sup	1_rod(sup	1_rod(sup	1_rod(sup	1_rod(sup	1_rod(sup	1_rod(sup	2_rod(sup	2_rod(sup	2_rod(su	
3	0.2001	-9.56295	551.229	6.84E-16	-1.02E-14	9.57E-17	1.71E-17	8.25158	9.56295	551.229	7.19E-16	1.02E-14	-3.41E-16	1.88E-17	8.25158	1.33E-16	541.667	-6.84E-16
4	0.4002	-9.5303	550.418	2.59E-16	-1.08E-14	-7.32E-16	-4.09E-20	8.25158	9.5303	550.418	4.38E-16	1.07E-14	-6.33E-16	-1.02E-18	8.25158	-5.83E-17	540.887	-1.50E-15
5	0.6003	-9.51692	549.064	1.86E-15	-8.04E-15	-9.93E-16	-3.85E-17	8.25158	9.51692	549.064	1.49E-15	8.08E-15	-8.71E-16	-8.00E-17	8.25158	-2.14E-16	539.547	1.55E-15
6	0.8004	-9.56988	547.17	3.03E-14	-5.21E-15	-9.83E-15	3.75E-15	8.25158	9.56988	547.17	2.99E-14	8.09E-15	6.04E-15	2.88E-15	8.25158	2.10E-14	537.6	-1.78E-14
7	1.0005	-9.50286	544.734	6.74E-15	1.09E-14	-3.44E-15	2.59E-14	8.25158	9.50286	544.734	5.76E-15	1.15E-15	8.96E-16	2.53E-14	8.25158	5.81E-14	535.231	-2.06E-13
8	1.2006	-9.55164	541.757	1.90E-14	-1.04E-14	-8.17E-15	3.40E-14	8.25158	9.55164	541.757	1.88E-14	4.54E-14	5.31E-15	3.52E-14	8.25158	1.59E-13	532.205	-2.99E-13
9	1.4007	-9.54461	538.238	1.80E-14	5.41E-14	-5.91E-15	5.16E-14	8.25158	9.54461	538.238	1.80E-14	6.76E-15	2.27E-15	5.27E-14	8.25158	2.69E-13	528.693	-4.49E-13
10	1.6008	-9.50651	534.178	5.36E-14	6.13E-14	-6.07E-15	5.41E-14	8.25158	9.50651	534.178	5.34E-14	-8.86E-15	3.91E-15	5.45E-14	8.25158	2.33E-13	524.672	-4.47E-13
11	1.8009	-9.57138	529.577	2.69E-14	3.34E-14	6.21E-15	6.76E-14	8.25158	9.57138	529.577	2.67E-14	1.99E-14	-6.68E-15	6.77E-14	8.25158	2.43E-13	520.006	-6.24E-13
12	2.001	-9.511	524.434	1.42E-14	5.96E-14	1.30E-14	7.14E-14	8.25158	9.511	524.434	1.39E-14	3.13E-14	-1.24E-14	7.05E-14	8.25158	4.19E-13	514.923	-6.07E-13
13	2.2011	-9.53779	518.75	1.10E-14	5.94E-14	1.15E-14	7.22E-14	8.25158	9.53779	518.75	9.77E-15	5.87E-14	-1.20E-14	7.13E-14	8.25158	5.59E-13	509.213	-6.68E-13
14	2.4012	-9.5575	512.525	2.53E-14	1.06E-13	2.88E-15	8.65E-14	8.25158	9.5575	512.525	2.40E-14	6.38E-14	-2.21E-15	8.65E-14	8.25158	7.87E-13	502.968	-8.32E-13
15	2.6013	-9.50079	505.758	2.71E-16	1.07E-13	-1.43E-15	9.18E-14	8.25158	9.50079	505.758	-5.88E-15	6.38E-14	5.01E-16	9.07E-14	8.25158	8.23E-13	496.258	-8.49E-13
16	2.8014	-9.56717	498.45	-2.01E-14	9.52E-14	-4.46E-15	9.01E-14	8.25158	9.56717	498.45	-8.44E-15	8.61E-14	2.96E-15	9.25E-14	8.25158	8.92E-13	488.883	-8.64E-13
17	3.0015	-9.52311	490.601	3.27E-15	9.52E-14	-1.58E-15	9.59E-14	8.25158	9.52311	490.601	1.52E-15	8.86E-14	-2.22E-15	9.59E-14	8.25158	8.76E-13	481.078	-8.93E-13
18	3.2016	-9.52362	482.211	1.16E-14	9.72E-14	-4.44E-15	9.79E-14	8.25158	9.52362	482.211	1.03E-14	9.03E-14	1.67E-16	9.78E-14	8.25158	8.79E-13	472.687	-9.34E-13
19	3.4017	-9.5669	473.279	7.28E-16	9.16E-14	-5.70E-15	1.03E-13	8.25158	9.5669	473.279	-1.30E-15	1.02E-13	2.11E-15	1.03E-13	8.25158	9.17E-13	463.712	-9.71E-13
20	3.6018	-9.50069	463.805	-9.07E-16	9.71E-14	-7.35E-15	1.05E-13	8.25158	9.50069	463.805	-3.06E-15	9.81E-14	3.70E-15	1.05E-13	8.25158	9.34E-13	454.305	-9.73E-13
21	3.8019	-9.55792	453.791	7.55E-15	9.69E-14	-8.46E-15	1.05E-13	8.25158	9.55792	453.791	3.82E-15	1.06E-13	5.92E-15	1.05E-13	8.25158	9.62E-13	444.233	-1.00E-12
22	4.002	-9.53725	443.235	7.64E-15	9.82E-14	-1.15E-14	1.03E-13	8.25158	9.53725	443.235	4.04E-15	1.02E-13	6.41E-15	1.02E-13	8.25158	9.38E-13	433.697	-9.59E-13

Figure 22: A snapshot of the CSV File with data logs

MATLAB was then used to process the data file to extract data of interest. Using commands included in Appendix I that used the logged extension to calculate the strains in each cable. The maximum strain experienced was extracted for each of the 24 cables, shown below in Figure 23.

1	0.0177	13	0.0178
2	0.0178	14	0.0178
3	0.0178	15	0.0208
4	0.0178	16	0.0208
5	0.0178	17	0.0208
6	0.0178	18	0.0208
7	0.0178	19	0.0180
8	0.0177	20	0.0180
9	0.0178	21	0.0180
10	0.0178	22	0.0180
11	0.0178	23	0.0177
12	0.0178	24	0.0177

Figure 23: Calculated Maximum Strains for each cable.

Literature states 1080 Spring Steel can experience strain before breakage to about 12% [28] [29], from the obtained results, the maximum strain observed by the cables was during impact upon landing only reaching a maximum of 2%.

Additionally, the data from NTRT and MATLAB were further used to produce plots for the kinematic analysis of all the struts in the structure, results for one of which can be seen in Figure 24; the result for the rest of the struts are similar and are included in Appendix II. Through literature it is know that the 6061-T6 Aluminium alloy struts are capable of sustaining acceleration up to 25G justifying the kinematic analysis which concludes the struts in the structure in the given configuration only experience up to 3G's of acceleration.

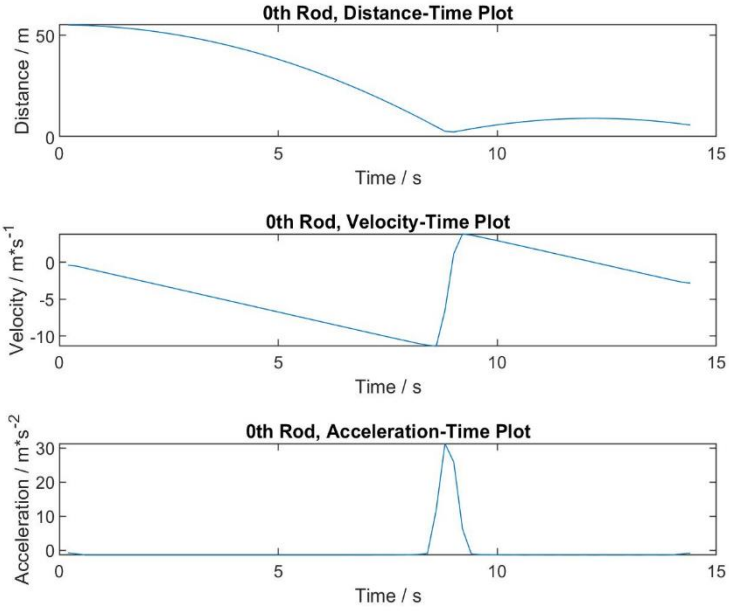

Figure 24: Kinematic Analysis for the 0th Strut

Finite Element Analysis on COMSOL

The initial finite element model was calibrated using simulation results available from NASA. The calibration parameters included spring constant, strut diameters and spring pre-tension. The results of the calibrated model are given below:

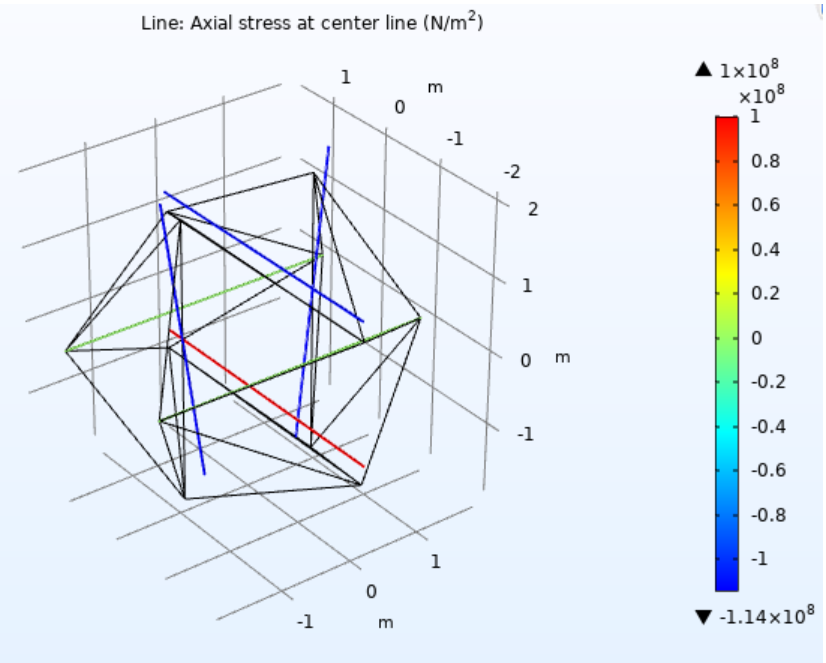

Figure 25: Result of Analysis on COMSOL

The compressive stress in this case was around 114 MPa, which is similar to NASA's 100 MPa. Finite Element Analysis gave a conservative result that may be attributed to the limitations of model.

After validating the setup, the configuration summarized in Table 2 was tested.

Table 2: Initial Specifications

Strut Diameter	3.175 cm
Spring Constant	220 kN/m
Pre-Tension	8800 N

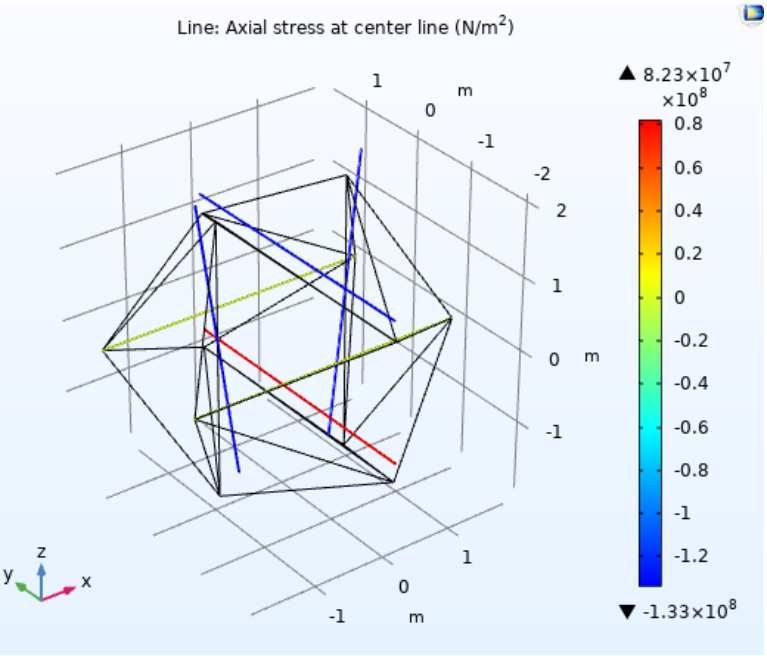

Figure 26: Analysis results for Initial Specifications

The value of pre-tension and spring constant was chosen using iterative simulations on NTRT and COMSOL, based on the decided strut and cable materials, as well as the strut length of 3.8 m. Running the simulation, the struts were found to be under a compressive stress of 133 MPa as shown in Figure 26. The yield stress of 6061-T6 Aluminium at Titan's temperature of -175 C, is around 320 MPa [30] [31]. Therefore, the FOS was around 2.4 that was well above the target FOS of 2. Thus, the diameter of the strut was decreased to optimize the design.

Optimization

In order to decrease the weight of the robot as much as possible, the diameter of the rod was decreased while keeping the target FOS of 2 in mind. Decreasing the strut diameter to 2.8 cm, resulted in compressive stresses of 171 MPa and an FOS of 1.87, shown in Figure 27.

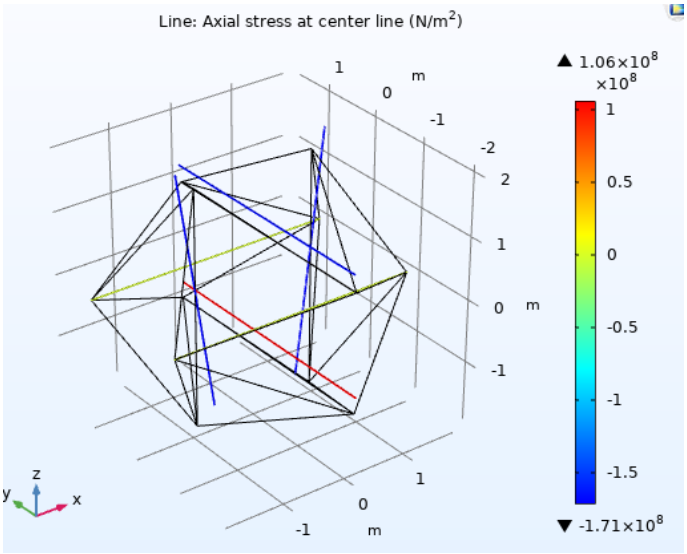

Figure 27: Analysis Results for Diameter = 2.8 cm

Increasing the strut diameter slightly to 3 cm, resulted in peak compressive stresses of about 150 MPa, as can be seen in Figure 28, and therefore a FOS of 2.15. As this FOS was near our desired FOS and was on the safer side of it, therefore the strut diameter was optimized to a value of 3 cm.

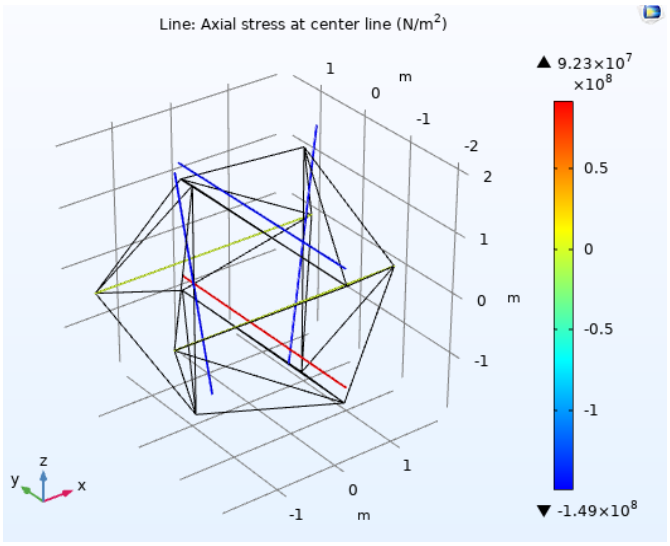

Figure 28: Analysis Results for Diameter = 3 cm

Eigenfrequency Analysis on COMSOL

Having fixed the strut length and diameter as well as the spring's constant and pre-tension, the eigenfrequency analysis was then performed on the structure to determine the natural frequencies.

The analysis resulted in 36 natural frequencies, tabulated in Figure 29.

% Eigenfrequency (Hz)	
1.01368454706014E-06i	60.63169895
1.57644885572285E-6i	60.79031277
1.42E-06	62.15727866
10.30883013	69.37151758
11.44466644	70.71343248
11.44725111	77.9680331
11.48893698	78.01032057
29.55233547	78.80461514
29.96976705	105.2731803
30.16333129	105.4291044
36.65392452	105.7146921
36.90651933	117.9715007
37.05782794	741.9125447
38.90911823	742.0142447
40.90762685	744.051428
51.82318905	744.0940815
52.19612091	744.2155167
52.71194208	748.0342804

Figure 29: Natural Frequencies found through Eigenfrequency

Although the selection of natural frequencies that are to be used for actuation are determined by experiments, the mode shape can give an insight into the direction that the structure would actuate/locomote in. The first three modes in Figure 29 correspond to rigid body motion and are thus neglected. Based on the mode shapes, 3 frequencies were selected: 11.4 Hz, 30.2 Hz, 60.3 Hz. In the figures 30, 31 and 32, the structure in purple shows the mode shape, while the structure in red shows the original, non-resonated structure.

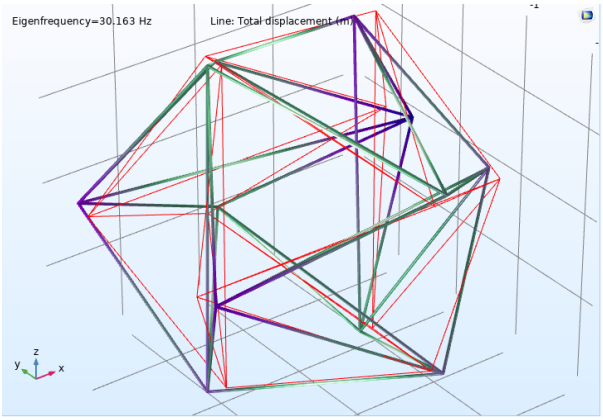

Figure 30: Mode shape for 30.2 Hz

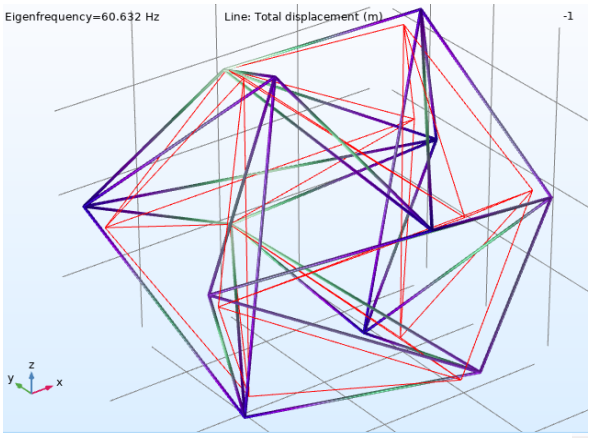

Figure 31: Mode shape for 60.3 Hz

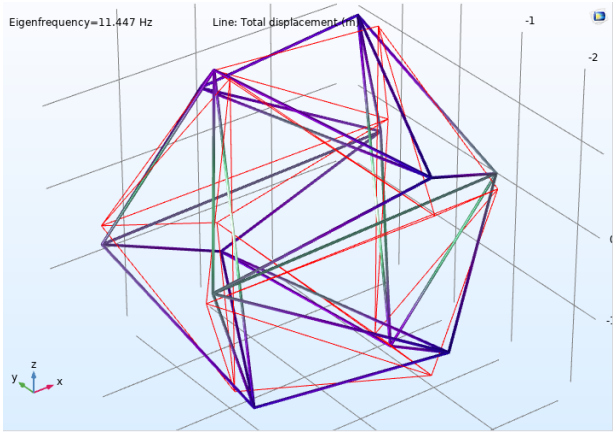

Figure 32: Mode shape for 11.4 Hz

Proof of concept

As mentioned earlier, to support the selection of our configuration and control system, it was decided to put together a simplified structure as a proof of concept. With the help of this structure, a clear justification and explanation of the chosen selection was possible. Figure 33 and 34 exhibit the model in the best and worst landing cases respectively.

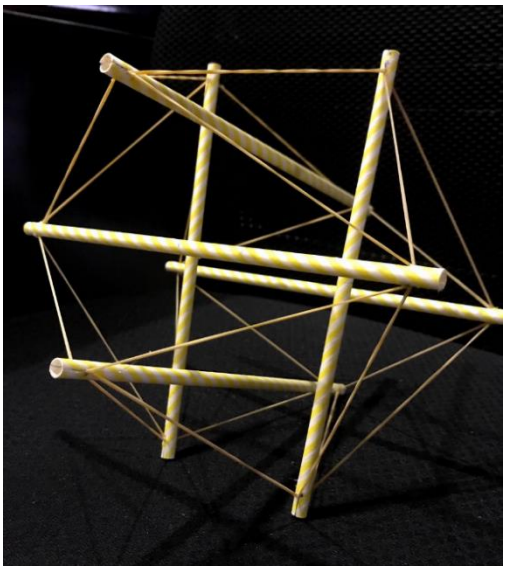

Figure 33: Proof of concept at 3 Point Landing (Best-case scenario)

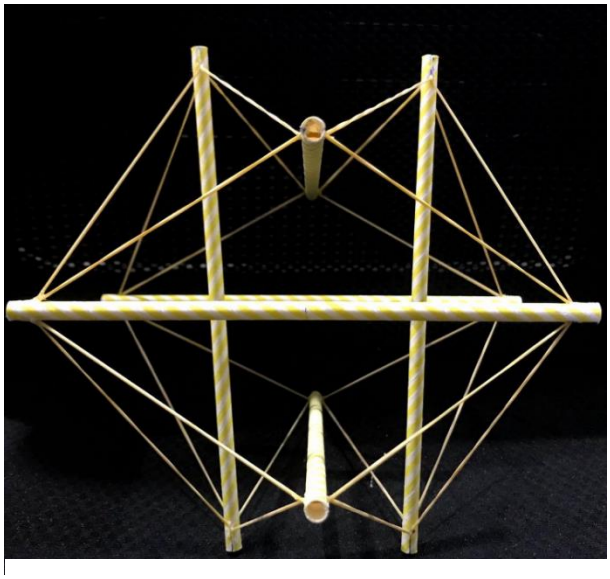

Figure 34: Proof of concept at 2 Point Landing (Worst-case scenario)

The details of the eccentric rotating mass vibrating motors, displayed in Figure 35, that were attached to the struts on the physical model as part of the chosen locomotion system are as follows:

Operating Voltage: 2.2-4 VDC

RPM: 2500

Dimensions: (12 x 6 x 3.6) mm

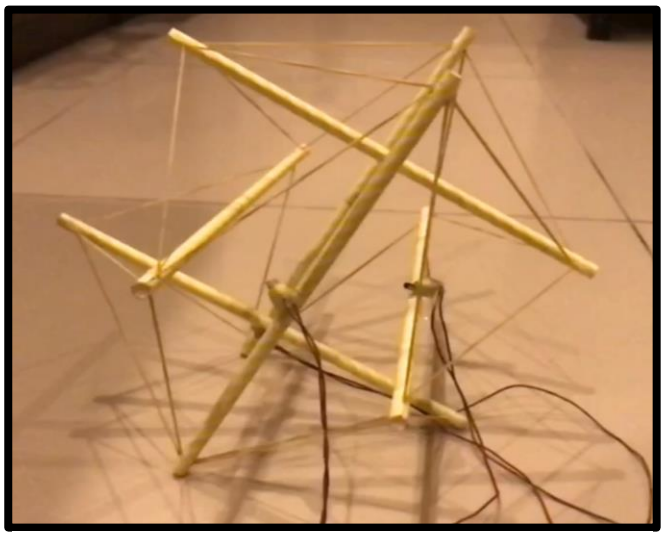

Figure 35: Motors attached on the Structure.

Final Design

The final design and specifications, after the literature review and consequent simulations, are summarized in Table 3.

Table 3: Summary of Final Specifications

Struts	Cables	Control System
6 Struts arranged as Icosahedron. Strut Length = 3.8 m Strut Diameter = 3 cm Strut Material: 6061-T6 Aluminium	24 cables Spring Constant = 220 kN/m Pre-tension = 8800 N Cable Material: 1080-Spring Steel	Open Loop Actuation System Actuation through vibration (morphological computation) Natural Frequencies used: 11.4 Hz, 30.2 Hz, 60.6 Hz

CHAPTER 5: CONCLUSION AND RECOMMENDATION

It was SunSpiral's & Agogino's research and claim of the tensegrity robot having no single point of failure, no axles or hinges that needed to be reinforced to withstand impact stresses which gave us the determination to explore the concept and implementation of tensegrity structures in space missions and the hope to develop a better insight of the changing requirements of space missions in order to further strengthen the standing of tensegrity robots as successful space probes. Working on this project for the past year, following is a list of the conclusions drawn from the extensive research and work:

1. Tensegrities are effective and reliable mobility and landing platforms with the ability to carry heavy science payloads without increasing the overall mass of the structure.
2. These systems can be used in varied terrains, with just differences in material selection based on the atmosphere of the target extra-terrestrial object.
3. The individual struts experiencing loads exceeding the Euler critical load does not imply structural failure, rather becomes a means for the structure to deform and store the elastic strain energy, which can be dissipated later on, in secure ways.
4. Impact stresses of the structure, at an impact velocity under consideration for Titan's atmosphere, were validated against NASA's results, along with the calculation of stresses for the structure designed by the group on COMSOL and the NTRT simulator.
5. A small prototype was developed as a proof of concept which facilitated an understanding of the extent of specification changes required for an improved version.

Recommendations

While significant progress on the project was made, the group was able to recognize the further avenues that have opened up for further research and exploration (appreciate the choice of word) that can be explored by future groups to develop the technology even further:

1. Simulating the actuation system in NTRT

   NASA made use of a control system that relied on cable colocation, and therefore released libraries that supported the particular choice of control system. As of yet and to the best of our knowledge, NTRT does not currently have a library that can be used directly to implement the vibration-based actuation system. Future groups can look into designing codes that can implement this choice of actuation systems.

2. Simulating the actuation system on rough terrains

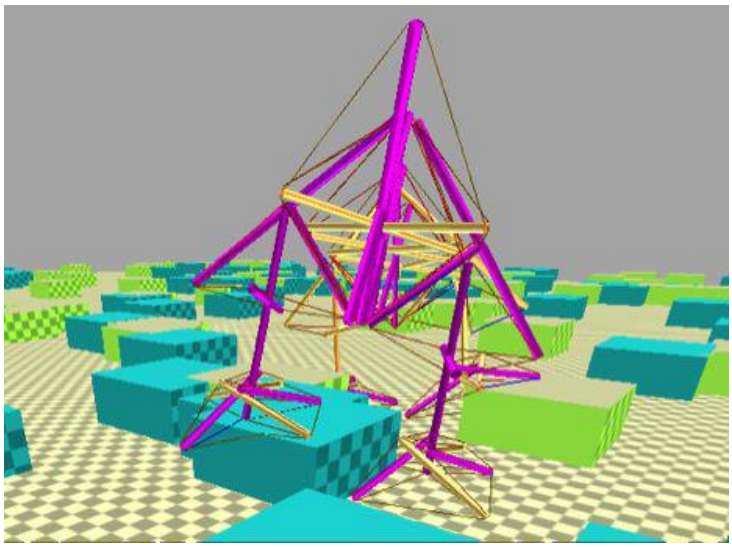

Figure 36: Navigating Rough Terrain in NTRT [4]

   NTRT allows the terrain to be altered by adding slopes (to imitate hills / uneven surfaces) as well as adding objects analogous to obstacles. Once the actuation system has been simulated in NTRT, the terrain's features can be changed to measure the effectiveness of the actuation system against each type of obstacle.

3. Prototyping

   Due to the COVID-19 pandemic, the group could not, unfortunately, manufacture their design and were limited to implementing the structure as well as the control system as the

proof of concept. Prototyping would open up a number of avenues into different experimentations that can be performed e.g., drop testing, comparison with simulations etc.

4. Use of Artificial Intelligence as part of control system
   NASA as well as other researchers made use of AI as part of the control system, in order to find the optimum parameters for their control system. This was done to avoid explicitly modelling the complex dynamics of the structure. AI algorithms can be used with any choice of actuation system to find the optimum strategy (specific to the actuation system) for smooth locomotion.

5. Use of Euler Lagrange Simulator
   NASA used the Euler Lagrange Simulator alongside NTRT to simulate their structures. Euler Lagrange simulator is a more accurate alternative to COMSOL, to model tensegrity structures.

6. Removing the need for aeroshells
   Aeroshells act as the only one-time use loads, still needed by tensegrity robots, that are discarded after entry and serve no further purpose in the mission. Removing them would not only reduce the non-scientific load of each mission, but additionally would remove the upper limit on strut length. Alternative technologies can be looked at which remove the need for aeroshells.

REFERENCES

[1] A. Pugh, An Introduction to Tensegrity, Univ. California Press, 1976.

[2] N. Bel Hadj Ali, L. Rhode-Barbarigos, A. A. Pascual Albi and I. F.C. Smith, "Design optimization and dynamic analysis of a tensegrity-based footbridge," *Applied Computing and Mechanics Laboratory, Ecole Polytechnique Fédérale de Lausanne (EPFL), ENAC/IIC/IMAC, Station 18, 1015 Lausanne, Switzerland,* 2010.

[3] V. S. D. A. Adrian Agogino, "Super Ball Bot - Structures for Planetary Landing and Exploration," NASA Ames Research Center, Intelligent Systems Division, 2013.

[4] A. A. D. A. Vytas SunSpiral, "Super Ball Bot - Structures for Planetary Landing and Exploration," NASA Ames Research Center, Intelligent Systems Division, 2015.

[5] R. W. C. R. J. B. R. D. Q. V. S. Brian R. Tietz, "Tetraspine: Robust Terrain Handling on a Tensegrity Robot Using Central Pattern Generators," in *IEEE/ASME International Conference on Advanced Intelligent Mechatronics (AIM)*, Wollongong, 2013.

[6] J. J. Rimoli, "On the impact tolerance of tensegrity-based planetary landers," in *AIAA Structures, Structural Dynamics, and Materials Conference*, San Diego, California, 2016.

[7] N. Science, "Entry, Descent, and Landing," NASA, [Online]. Available: https://mars.nasa.gov/mars2020/timeline/landing/entry-descent-landing/. [Accessed 18 May 2021].

[8] C. Paul, H. Lipson and F. J. V. Cuevas, "Evolutionary form-finding of tensegrity structures.," in *Proceedings of the 2005 Genetic and Evolutionary Computation Conference (GECCO)*, 2005.

[9] C. Paul, W. Roberts, H. Lipson and F. J. V. Cuevas, "Gait production in a tensegrity based robot.," in *Advanced Robotics, 2005. ICAR '05. Proceedings., 12th International Conference on*, 2005.

[10] C. Paul, F. J. V. Cuevas and H. Lipson, "Design and control of tensegrity robots for locomotion," *IEEE Transactions on Robotics,* 2006.

[11] A. P. Sabelhaus, H. Ji, P. Hylton, Y. Madaan, C. Yang, A. M. Agogino, J. Friesen and V. SunSpiral, "Mechanism Design and Simulation of the ULTRA SPINE, A Tensegrity Robot.," in *The ASME*

2015 International Design Engineering Technical Conferences And Computers and Information in Engineering Conference (IDETC/CIE 2015), Boston, 2015.

[12] S. Lessard, J. Bruce, A. Agogino, V. SunSpiral and M. Teodorescu, "Robust Monte Carlo Control Policies to Maneuver Tensegrity Robots out of Obstacles," in *Proceedings of Autonomous Robots and Multirobot Systems (ARMS)*, Istanbul, 2015.

[13] V. SunSpiral, R. D. Quinn and B. T. Mirletz, "CPGs for Adaptive Control of Spine-like Tensegrity Structures," no. National Aeronautics and Space Administration, NASA Ames Research Center, 2016.

[14] M. Khazanov, J. Rieffel and J. Jocque, "Developing morphological computation in tensegrity robots for controllable actuation," in *Annual Conference on Genetic and Evolutionary Computation*, 2014.

[15] M. Khazanov, B. Humphreys, W. Keat and J. Rieffel, "Exploiting Dynamical Complexity in a Physical Tensegrity Robot to Achieve Locomotion," in *ECAL 2013: The Twelfth European Conference on Artificial Life*, Sicily, 2013.

[16] J. W. R. H. L. F. J. V. C. Chandana Paul, "Gait Production in a Tensegrity Based Robot," Cornell University, Ithaca, 2005.

[17] H. C. Lee, A. M. Agogino, D. K. Lieu and R. S. Fearing, "Soft Spherical Tensegrity Robot Design Using Rod-Centered Actuation and Control. UC Berkeley," 2016.

[18] C. Paul, F. J. Valero-Cuevas and H. Lipson, "Design and Control of Tensegrity Robots for Locomotion," *IEEE TRANSACTIONS ON ROBOTICS,* vol. 22, no. 5, 2006.

[19] C. Paul, "Morphological computation A basis for the analysis of morphology and control requirements," *Robotics and Autonomous Systems,* no. 54, pp. 619-630, 2006.

[20] M. S. S. H. Yuusuke Koizumi, "Rolling Tensegrity Driven by Pneumatic Soft Actuators," in *IEEE International Conference on Robotics and Automation*, Minnesota, 2012.

[21] K. L. Q. H. S. C. Zhijan Wang, "A Light-Powered Ultralight Tensegrity Robot with High Deformability and Load Capacity," Advanced Materials, San Diego, 2019.

[22] M. Shibata, F. Saijyo and S. Hirai, "Crawling by Body Deformation of Tensegrity Structure Robots," *IEEE International Conference on Robotics and Automation,* 2009.

[23] W. B. Hubbard and B. Buratti, Britannica, [Online]. Available: https://www.britannica.com/place/Titan-astronomy/The-atmosphere.

[24] S. Mraz, “Basics of Aerospace Materials: Aluminum and Composites,” Machine Design, 19 June 2014. [Online]. Available: https://www.machinedesign.com/materials/article/21831769/basics-of-aerospace-materials-aluminum-and-composites.

[25] C. L. M. Peters, “Aerospace and Space Materials,” *MATERIALS SCIENCE AND ENGINEERING,* vol. III.

[26] “Aalco,” Aalco, [Online]. Available: https://www.aalco.co.uk/datasheets/Aluminium-Alloy-6061-T6-Extrusions_145.ashx.

[27] C. T. M. and J. J. Z. , “The 1.5 & 1.4 Ultimate Factors of Safety for Aircraft & Spacecraft- History, Definition and Applications,” *NASA Ames Research Center: National Aeronautics and Space Administration,* February, 2014.

[28] AZoM, “AZO Materials,” 2012. [Online]. Available: https://www.azom.com/article.aspx?ArticleID=6115.

[29] “MATWEB,” [Online]. Available: http://www.matweb.com/search/datasheet_print.aspx?matguid=37ca3458dfbe482fbe1efdf59d52e424.

[30] W. Material, “AL 6061-T6 Aluminum Alloy Properties, Density, Tensile & Yield Strength, Thermal Conductivity, Modulus Of Elasticity, Welding,” The World Material, [Online]. Available: https://www.theworldmaterial.com/al-6061-t6-aluminum-alloy/. [Accessed 10 May 2021].

[31] “MatWeb,” [Online]. Available: http://www.matweb.com/search/DataSheet.aspx?MatGUID=b8d536e0b9b54bd7b69e4124d8f1d20a&ckck=1.

[32] “Vrije Universiteit Brussel,” [Online]. Available: http://lucy.vub.ac.be/gendes/actuators/muscles.htm.

[33] D. Stamenović and M. F. Coughlin, “A Quantitative Model of Cellular Elasticity Based on Tensegrity,” *Journal of Biomechanical Engineering,* pp. 39-43, 2000.

[34] J. Rieffel and J.-B. Mouret, “Adaptive and Resilient Soft Tensegrity Robots,” *Soft Robotics,* 2018.

[35] S. Fivat, J. Rieffel, C. Paul, F. Valero Cuevas and H. Lipson, “Tensegrity Robots,” Creative Machines Lab- Columbia University, [Online]. Available: https://www.creativemachineslab.com/tensegrity.html.

[36] 2. B. F. 9.-S. T. G. Dome, “Liveauctioneers,” [Online]. Available: https://www.liveauctioneers.com/item/6871769_208-buckminster-fuller-90-strut-tensegrity-geo-dome.

[37] Y. Zhao, S. Zhou, C. Lin and D. Li, “An Efficient Locomotion Strategy for Six-strut Tensegrity Robots,” in *13th IEEE International Conference on Control & Automation (ICCA)*, Ohrid, Macedonia.

[38] I. Designs. [Online]. Available: https://intensiondesigns.ca/tensegrity-modules/.

[39] “12 Strut Tensegrity,” Stanford University, Manuscripts Division, [Online]. Available: https://oac.cdlib.org/ark:/13030/kt7h4nb44k/?layout=metadata&brand=oac4.

APPENDIX I: CODES

NTRT C++ Code

The following is the .cpp file for out Tensegrity model, which uses the YAML file (code previously written) as an input, written for the NTRT simulator:

```
/*
 * Copyright © 2012, United States Government, as represented by the
 * Administrator of the National Aeronautics and Space Administration.
 * All rights reserved.
 *
 * The NASA Tensegrity Robotics Toolkit (NTRT) v1 platform is licensed
 * under the Apache License, Version 2.0 (the "License");
 * you may not use this file except in compliance with the License.
 * You may obtain a copy of the License at
 * http://www.apache.org/licenses/LICENSE-2.0.
 *
 * Unless required by applicable law or agreed to in writing,
 * software distributed under the License is distributed on an
 * "AS IS" BASIS, WITHOUT WARRANTIES OR CONDITIONS OF ANY KIND,
 * either express or implied. See the License for the specific language
 * governing permissions and limitations under the License.
*/


/**
```

```
 * @file BuildTensegrityModel.cpp
 * @brief Contains the definition function main() for TensegrityModel
 * which builds a model based on tensegrity structure defined in YAML
 * @author Simon Kotwicz & Jonah Eisen
 * @edited by: Saad Shabeer, Mahnoor Bilal & Abdul Muhaimin Pandhiani
 * $Id$
 */

// This application
#include "TensegrityModel.h"
#include "TensegrityModelController.h"
// This library
#include "core/terrain/tgBoxGround.h"
#include "core/tgModel.h"
#include "core/tgSimulation.h"
#include "core/tgSimViewGraphics.h"
#include "core/tgWorld.h"
#include "sensors/tgDataLogger2.h"
#include "sensors/tgRodSensorInfo.h"
#include "sensors/tgSpringCableActuatorSensorInfo.h"
// #include "sensors/tgCompoundRigidSensorInfo.h"

// Bullet Physics
```

```
#include "LinearMath/btVector3.h"

// The C++ Standard Library

#include <iostream>

#include <string>

#include <vector>



/**

 * The entry point.

 * @param[in] argc the number of command-line arguments

 * @param[in] argv argv[0] is the executable name

 * @param[in] argv argv[1] is the path of the YAML encoded structure

 * @return 0

 */

int main(int argc, char** argv)

{

   // For this YAML parser app, need to check that an argument path was

   // passed in.

   if (argv[1] == NULL)

   {

     throw std::invalid_argument("No arguments passed in to the application. You need to specify which YAML file you wouldd like to build.");

   }

   // create the ground and world. Specify ground rotation in radians
```

```
const double yaw = 0.0;
const double pitch = 0.0;
const double roll = 0.0;
const tgBoxGround::Config groundConfig(btVector3(yaw, pitch, roll));
// the world will delete this
tgBoxGround* ground = new tgBoxGround(groundConfig);

const tgWorld::Config config(13.52); // gravity, dm/sec^2
tgWorld world(config, ground);

// create the view
const double timestep_physics = 0.0001; // seconds
const double timestep_graphics = 1.f/60.f; // seconds
tgSimViewGraphics view(world, timestep_physics, timestep_graphics);

// create the simulation
tgSimulation simulation(view);

// create the models with their controllers and add the models to
// the simulation.
// This constructor for TensegrityModel takes the "debugging" flag
// as its second parameter. Set to true, and the simulation will
// output lots of information about the model that's created.
```

```
TensegrityModel* const myModel = new TensegrityModel(argv[1], false);
/*
	Controller Section from App3BarYAML
*/

// Attach a controller to the model, if desired.
// This is a controller that interacts with a generic TensegrityModel as
// built by the TensegrityModel file.

// Parameters for the TensegrityModelController are specified in that .h file,
// repeated here:
double startTime = 45;
double minLength = 0.7;
double rate = 8;
std::vector<std::string> tagsToControl;

tagsToControl.push_back("actuated_string");

// Change horizontal_string to as needed

// Create the controller
TensegrityModelController* const myController = new
TensegrityModelController(startTime, minLength, rate, tagsToControl);
```

```
  myModel->attach(myController);


  /*
        END OF CODE FROM App3BarYAML
  */


  // Add the model to the world
  simulation.addModel(myModel);


  // For Data Logging
  // Source: https://github.com/NASA-Tensegrity-Robotics-Toolkit/NTRTsim/blob/master/src/dev/ultra-spine/SpineKinematicsTest/AppSpineKinematicsTest.cpp
  // Add sensors using the new sensing framework
  // A string prefix for the filename
  std::string log_filename = "/home/tensegribuntu/NTRTsim-master/src/examples/FYP_V1/Data_Logs/FYPTest1.csv";
  // The time interval between sensor readings:
  double timeInterval = 0.2;
  // First, create the data manager
  tgDataLogger2* myDataLogger = new tgDataLogger2(log_filename, timeInterval);
  //std::cout << myDataLogger->toString() << std::endl;
  // Then, add the model to the data logger
  myDataLogger->addSenseable(myModel);
  // Create sensor info for all the types of sensors that the data logger
```

```
    // will create.
    tgRodSensorInfo* myRodSensorInfo = new tgRodSensorInfo();
    tgSpringCableActuatorSensorInfo* mySCASensorInfo =
      new tgSpringCableActuatorSensorInfo();
    //tgCompoundRigidSensorInfo* myCRSensorInfo = new
tgCompoundRigidSensorInfo();
    // Attach the sensor infos to the data logger
    myDataLogger->addSensorInfo(myRodSensorInfo);
    myDataLogger->addSensorInfo(mySCASensorInfo);
    //myDataLogger->addSensorInfo(myCRSensorInfo);
    // Next, attach it to the simulation
    simulation.addDataManager(myDataLogger);

    //End of code for Data Logging

    simulation.run();

    // teardown is handled by delete
    return 0;
}
```

MATLAB Script for Kinematic Analysis of a single strut

```
Time = readtable('FYPTest.xlsx','Range','A2:A74');
Time = Time{:,:};
```

```
%-------------------------------Strut 0-----------------------------------%

Rod_0_X = readtable('FYPTest.xlsx', 'Range', 'B2:B74');

Rod_0_X = Rod_0_X {:,:};

Rod_0_Y = readtable('FYPTest.xlsx', 'Range', 'C2:C74');

Rod_0_Y = Rod_0_Y {:,:};

Rod_0_Z = readtable('FYPTest.xlsx', 'Range', 'D2:D74');

Rod_0_Z = Rod_0_Z {:,:};

Rod_0_Vector = (sqrt((Rod_0_X.^2)+(Rod_0_Y.^2)+(Rod_0_Z.^2)))/10;

Rod_0_Velocity = gradient(Rod_0_Vector(:))./gradient(Time(:));

Rod_0_Acceleration = gradient(Rod_0_Velocity(:))./gradient(Time(:));


%Plotting Graph

figure()

tiledlayout(3,1)


%Top Plot - Distance

ax1 = nexttile;
```

```
plot(ax1,Time,Rod_0_Vector)

xlabel(ax1, 'Time / s')

ylabel(ax1, 'Distance / m')

title(ax1, '0th Rod, Distance-Time Plot')


%Top Plot - Velocity

ax2 = nexttile;

plot(ax2,Time,Rod_0_Velocity)

xlabel(ax2, 'Time / s')

ylabel(ax2, 'Velocity / m*s^-^1')

title(ax2, '0th Rod, Velocity-Time Plot')


%Top Plot - Acceleration

ax3 = nexttile;

plot(ax3,Time,Rod_0_Acceleration)

xlabel(ax3, 'Time / s')

ylabel(ax3, 'Acceleration / m*s^-^2')

title(ax3, '0th Rod, Acceleration-Time Plot')
```

This code is then repeated for the other 5 struts.

MATLAB Commands to calculate maximum strain for a single cable

% code to extract strain for the 3rd Cable (Cable 8 in the CSV sheet, as 0 – 5 are struts)

Elongation8 = DataLog{:,9}-DataLog{:,8};

Strain8 = Elongation8./DataLog{:,8};

MaxStrain8 = max(Strain8)

APPENDIX II: KINEMATIC ANALYSIS RESULTS

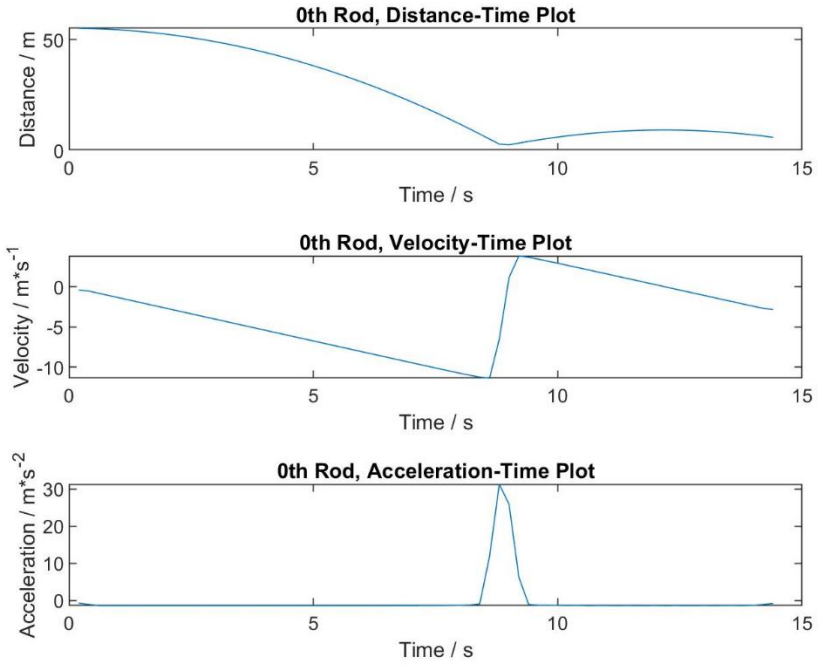

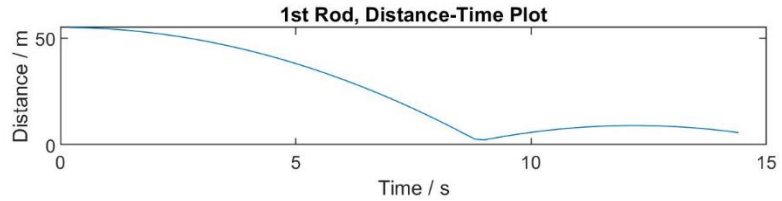
1st Rod, Distance-Time Plot
Distance / m
50
0
0
5
10
15
Time / s

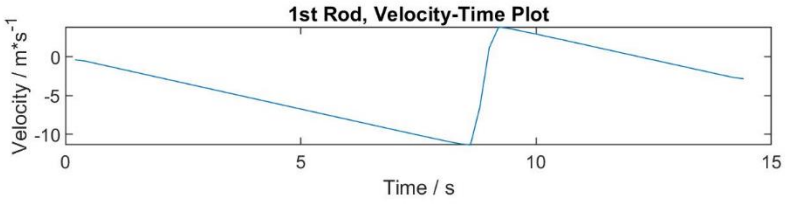
1st Rod, Velocity-Time Plot
Velocity / m*s-1
0
-5
-10
0
5
10
15
Time / s

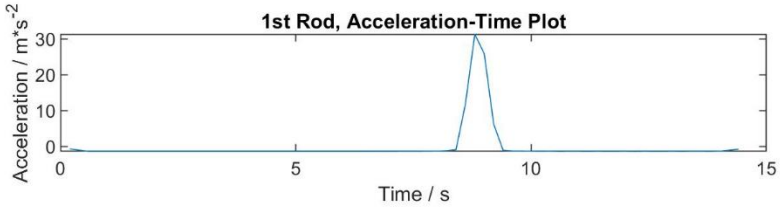
1st Rod, Acceleration-Time Plot
Acceleration / m*s-2
30
20
10
0
0
5
10
15
Time / s

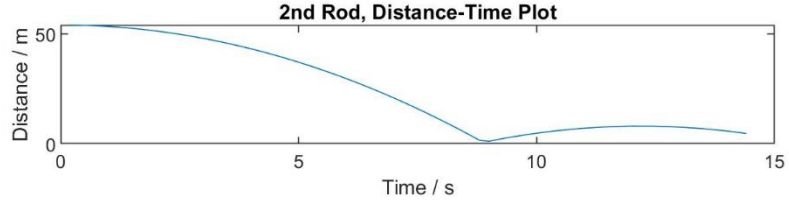
2nd Rod, Distance-Time Plot
Distance / m
50
0
0
5
10
15
Time / s

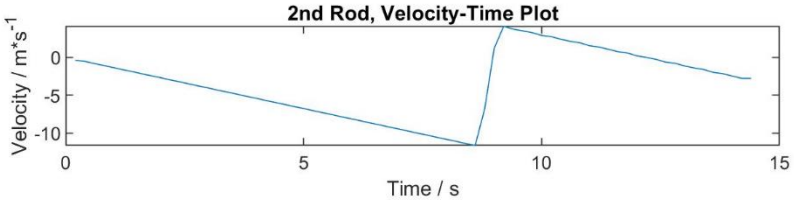
2nd Rod, Velocity-Time Plot
Velocity / m*s-1
0
-5
-10
0
5
10
15
Time / s

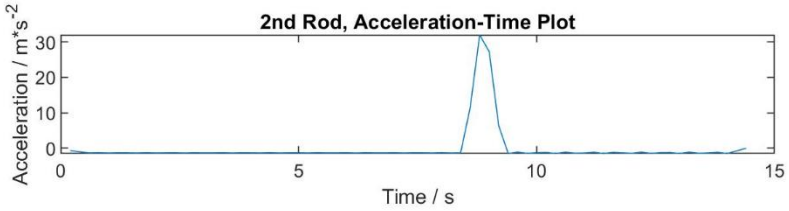
2nd Rod, Acceleration-Time Plot
Acceleration / m*s-2
30
20
10
0
0
5
10
15
Time / s

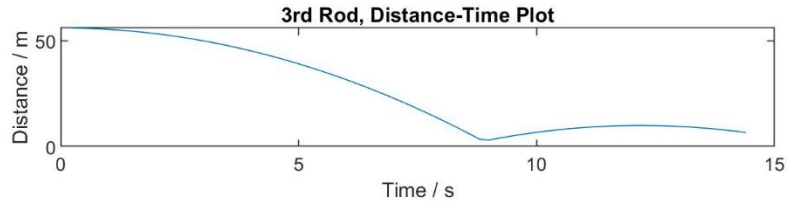
3rd Rod, Distance-Time Plot
Distance / m
50
0
0
5
10
15
Time / s

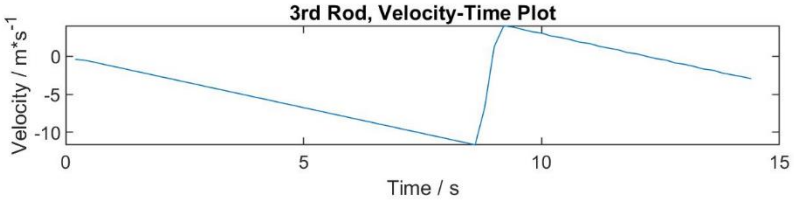
3rd Rod, Velocity-Time Plot
Velocity / m*s-1
0
-5
-10
0
5
10
15
Time / s

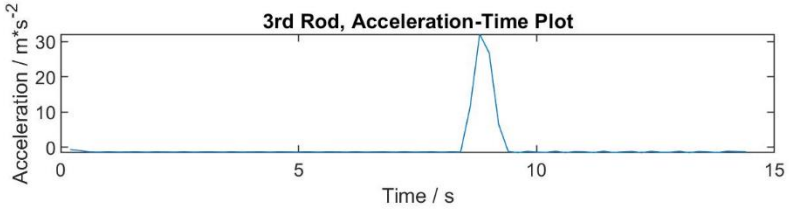
3rd Rod, Acceleration-Time Plot
Acceleration / m*s-2
30
20
10
0
0
5
10
15
Time / s

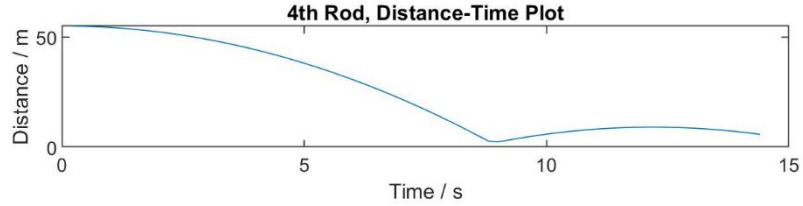
4th Rod, Distance-Time Plot
Distance / m
50
0
0
5
10
15
Time / s

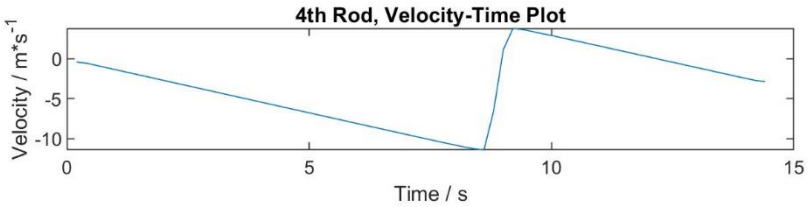
4th Rod, Velocity-Time Plot
Velocity / m*s-1
0
-5
-10
0
5
10
15
Time / s

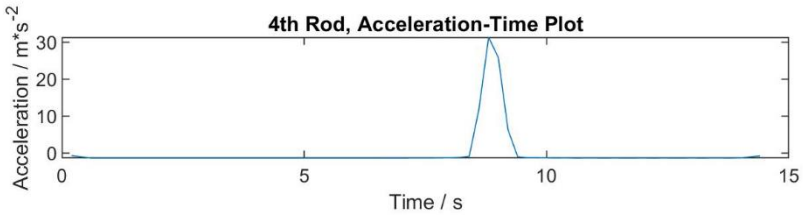
4th Rod, Acceleration-Time Plot
Acceleration / m*s-2
30
20
10
0
0
5
10
15
Time / s

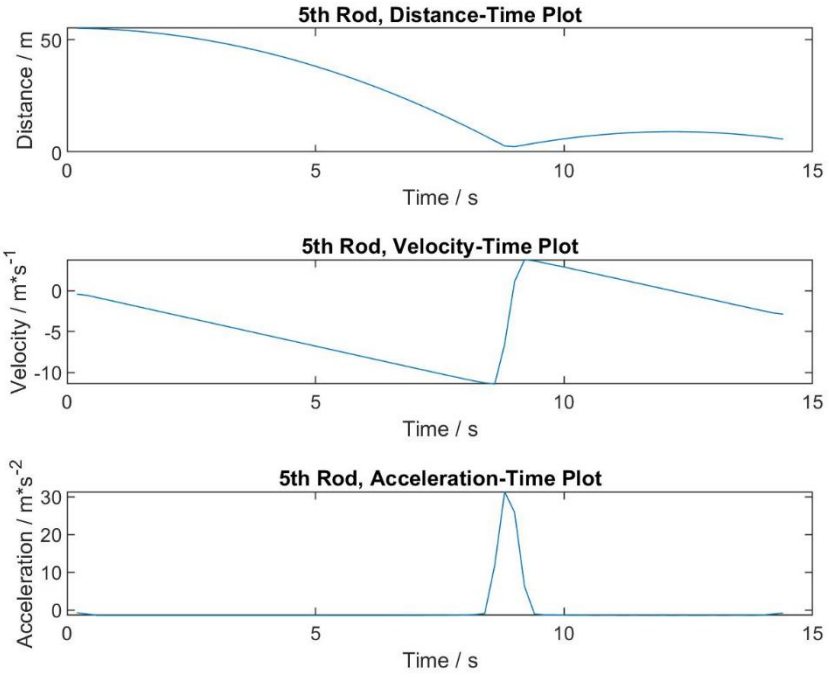

Figure 37: Kinematic Analysis plots for all 6 struts